ANL-6267

Argonne National Laboratory

DESIGN AND MASS TRANSFER STUDY FOR NEW MULTISTAGE FLUIDIZATION REACTOR

by

Kenneth Donald Williamson, Jr.

DISCLAIMER

LEGAL NOTICE

Price $2.75 . *Available from the Office of Technical Services, Department of Commerce, Washington 25, D.C.*

ANL-6267
Chemistry - General
(TID-4500, 15th Ed.)
AEC Research and
Development Report

ARGONNE NATIONAL LABORATORY
9700 South Cass Avenue
Argonne, Illinois

DESIGN AND MASS TRANSFER STUDY FOR NEW MULTISTAGE FLUIDIZATION REACTOR

by

Kenneth Donald Williamson, Jr.
Chemical Engineering Division

Based on a Thesis Submitted to the Faculty of
The Pennsylvania State University
in Partial Fulfillment of the Requirements for the
Degree of Doctor of Philosophy

December 1960

Operated by The University of Chicago
under
Contract W-31-109-eng-38

ACKNOWLEDGEMENT

This work would not have been possible without the advice, assistance and encouragement of many individuals at The Pennsylvania State University and the Argonne National Laboratory. In particular, I wish to acknowledge the help of the following:

The Laboratory for its complete financial support of the work and Dr. H. K. Schilling for abating the University fee requirements; Dr. E. T. Williams and Dr. Arthur Rose for their patience, encouragement and most helpful guidance throughout the project; Professors M. R. Cannon, W. A. Lloyd and W. W. Miller for serving on my committee; Mr. A. A. Jonke for advice and numerous valuable suggestions; Mr. V. H. Munnecke for help with administrative arrangements; Messrs. I. E. Knudsen and L. O. Mead for aid in obtaining equipment; Mr. N. M. Levitz for general assistance as Leader of the Fluidization Group; Messrs. W. J. Voss and T. L. Denst for excellent shop work; Messrs. J. D. Artzen, M. S. Jones, D. J. Raue, E. F. Johnston and J. E. Kincinas for operational help and advice from time to time; Graphic Arts for preparing the graphs and figures and for doing the Multilith reproduction work; Mrs. S. P. Colaric and Miss C. J. Holloway for excellent typing of the manuscript; and especially to my wife who has been a constant source of inspiration and encouragement.

CONTENTS

I. SUMMARY

A. Statement of the Problem

Multistage fluidization reactors in use today are generally equipped with downcomers to permit the movement of solids from stage to stage. However, this method of achieving downward transport of solids results in unstable column operation. To overcome this problem a method was developed by this author which eliminated downcomers and achieved downward transport of solids by utilizing vibration to "shake-down" the fluidized material through a plate consisting of large, non-fluidized, spherical beads and a support screen. It was the purpose of this work to improve the preliminary plate design, build a three-stage six-inch diameter column and to obtain and correlate design and mass-transfer data using the new equipment.

B. Procedure

For the design study the glass-bead air system was used. The data were evaluated on the basis of the effect that changes in the variables had upon the solids throughput rate. This rate was determined as a function of (1) vibrator size and vibrational frequency (6000 to 10000 CPM), (2) feed particle size (0.0030 to 0.0110 in. diameter), (3) plate resistance (depth, density and diameter of the large non-fluidized beads), (4) superficial air velocity (zero to 0.5 ft/sec) and (5) fluidized bed depth (3 to 9 in.).

For the mass-transfer study, the silica-gel water-vapor adsorption system was chosen because it lends itself readily to the fluidization technique and presents no difficult analytical problems. The equilibrium relationship for the system was determined for temperatures from 20 to 40°C and pressures from atmospheric to 20 psia.

These data were then used to evaluate the Murphree vapor efficiency for the adsorption of water vapor from air by silica gel in the six-inch diameter multistage unit. From the efficiency a modified mass-transfer coefficient was calculated. Runs were made at bed depths from 3/4 in. to 8 in. and superficial air velocities from 0.20 to 0.98 ft/sec.

C. Results and Conclusions

Two improvements were made on the preliminary plate design. The first was the incorporation of a cover screen as part of each plate. This in effect "sandwiched" the large non-fluidized beads and resulted in greatly improved operational stability. The second improvement was the use of internal vibration. This advance permitted control of the fluidized solids bed depth on an individual stage basis.

All of the design data were correlated into a set of five equations. These equations account for variations in feed particle density, shape and size; column cross sectional area; density and superficial velocity of the fluidizing gas; and the amount and size of the non-fluidized beads on the distributor plate. From the equations it is possible to calculate the amount and size of non-fluidized beads that are necessary to achieve a given throughput rate of any material under any operating conditions. The correlation was tested by making runs using non-spherical alumina and silica gel feeds.

In the mass-transfer study the Murphree vapor efficiency was found to be approximately 100% for all bed depths investigated and for all but the highest superficial air velocity. At an air velocity of 0.98 ft/sec the efficiency dropped to 96.5% corresponding to a modified mass-transfer coefficient of 35.4 $lb/sec\text{-}ft^3\text{-}lb/ft^3$.

The high efficiencies could not be attributed to the equipment design but rather to the fact that the gel particles were small and would have been efficient in any type of equipment when tested under the operating conditions used in this study.

II. INTRODUCTION

A. General Discussion

Since 1945 the fluid-bed technique for contacting fluids and solids has found widespread application in the chemical and petroleum processing industries. A fluidized bed results from the passage of a fluid upward through a bed of small, particulate solids at a velocity sufficiently high to impart a buoying effect to the solids. The fluid used can be either liquid or gas. In the case of liquids the fluidization is referred to as particulate; in the case of gases as aggregative.

There are several stages of fluidization which are dependent upon the velocity of the fluidizing medium and the particle movement within the bed. In the initial stage the bed expands but no significant circulatory motion is imparted to the particulate solids. As the velocity of the gas is increased a point of minimum fluidization is reached. Under this condition, bubbles appear on the surface of the bed and there is a limited amount of particle circulation. Further increases in gas velocity result in increased bed turbulence. At very high fluid velocities the bed becomes dispersed and is carried from the equipment in the fluid stream.

In general, the operating conditions used for industrial applications are characterized by high turbulence in which the solids move upward through the center of the bed and downward along the walls of the equipment. This is the result of the fact that the highest fluid velocities occur in the middle of the bed.

In conclusion, it can be stated that fluidization occurs between the extremes of fixed bed operation, in which the solids are

fixed in position, and pneumatic transport of solids, in which the fluid velocity is high enough to carry the particulate solids in the fluid stream.

Prior to 1940 fluidization techniques were confined to the separation of solids of different densities, particularly in the mineral industry. This was typically done by suspending the solids in a rising stream of water[9]. At the time it was considered impossible to suspend solids by gases.

The rapid development of the latter technique was the result of the petroleum industry's search for better methods to process crude oils. A pioneer in the development of catalytic cracking as an application of the fluid-bed process was the Standard Oil Development Co.[26,27]. This early work was an outgrowth of the fixed-bed method for catalytic cracking.

The use of a standpipe for transfer of solids was soon developed[29]. This, combined with the fluid bed, a transfer line, and a solids recovery system represents the basic fluid-bed system as it is known today.

The literature is filled with reports of work investigating the mechanics and basic (solid and fluid) parameters involved in fluidization[5,14,17,21,22,24,36,38]. Considerable data is also reported on chemical applications involving batch or single stage processing[18, 19,20]. Because of the turbulence within a fluidized bed, uniform temperature is maintained throughout. This has led to interest in the field of heat transfer with the resultant publication of many papers on the subject[1,13,23,34,35].

B. Multistage Work

In certain applications, it is desirable to maintain axial temperature and concentration gradients within the reacting material. Because of the turbulent nature of fluidized beds, this is not possible where only one stage is involved. For such situations, multistage reactors have been developed.

Levey, Jr., et al.[16] have developed a single-stage reactor which has the advantages of the multistage units. Their design incorporates tapered columns to hold the fluidized bed. As a direct result of the taper, solids mixing is reduced by a factor of ten, thus leading to true countercurrent operation.

At the present time, all industrial multistage units accomplish downward transport of solids between stages by means of plates and downcomers. Industrial applications utilizing such units include the magnetic conversion of iron ores[31], the adsorption separation of hydrocarbon gases with charcoal[7], the recovery of dilute oxides of N_2[6], the methylation of pentanes[28], the conversion of UO_3 to UF_4[10] and the dehumidification of air[3]. Downcomers have caused the most difficulty in the operation of such units because of back-mixing resulting from slugging in the downcomer tubes. This has led to unstable operation[6,11].

C. Present Work

In work at The Pennsylvania State University[37], a method to achieve downward transport of solids without downcomers was devised. Two major developments were responsible for the success of this work. The first was the discovery that proper fluidization could be achieved above a simple supporting screen if a layer of spherical beads that the

screen would not pass were incorporated in the bottom of the bed. The second major development was the utilization of vibration to "shake-down" the fluidized beads through the large beads and screen.

The promising results of the Pennsylvania State University work led to the present study which was carried out at the Argonne National Laboratory. Improvements were made on the original plate design and a three-stage, pilot-plant column was constructed. The experimental work fell into two areas: (1) development of a design correlation using the glass-bead air system, and (2) investigation of column efficiency from mass-transfer experiments involving the adsorption of water vapor from air by silica gel.

III. THE EQUIPMENT

A. Description

1. Multistage Column

A six-inch diameter column (Figures 1, 2) was constructed of alternate Pyrex glass pipe and brass sections with each of its three plates 24 inches apart. The glass permitted visual observation of the fluidized bed. Sample ports and pressure taps were located in the brass portions of the column.

The fluidizing gas entered at the bottom through the side of a glass tee and was uniformly distributed by passage through tightly packed cotton gauze. The gas left the column through two porous, sintered stainless steel filters. These trapped any entrained solids.

The feed was stored in a hopper located above the column. Gravity flow carried the material into a screw feeder and thence into the column at a point four inches from the top. The product was removed from the bottom through a manually-operated gate valve.

2. Plates

Each of the three plates consisted of three parts -- a support, a layer of beads, and a cover (Figure 3 and 4). The support and cover were identical and consisted of a wire screen attached to a punched-metal plate, the latter to add stiffness. Between the support and cover there was a layer of spherical beads. These beads offered resistance to the downward transport of solids. Because of their chemical and physical inertness, these will hereafter be referred to as inert beads. The openings in the cover and support were not large enough to permit the inert beads to escape. Vibration was transmitted

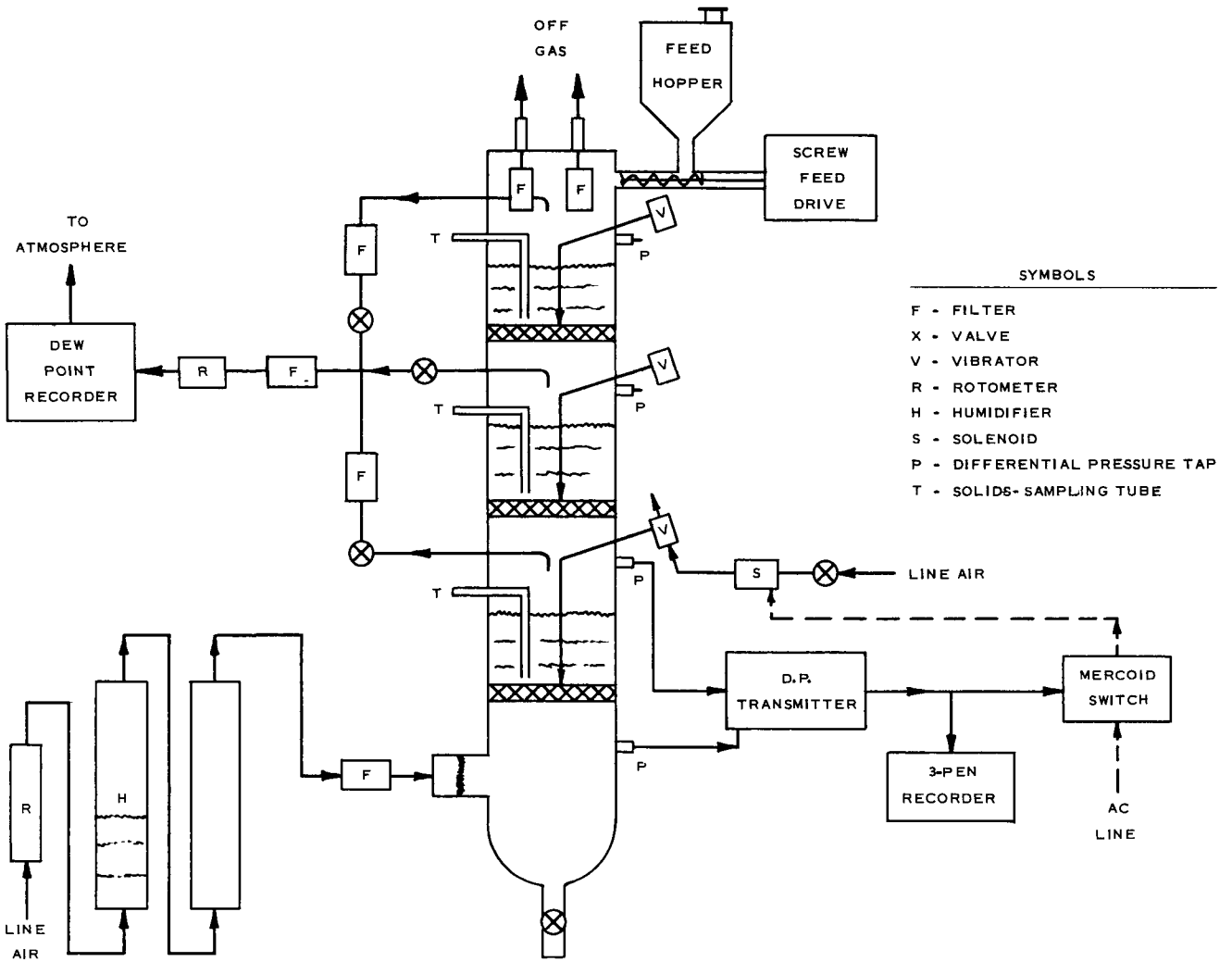

Figure 1. Schematic Diagram of the Multistage Fluidization Column with the Level Control System Shown for the Bottom Stage (all three stages were identical)

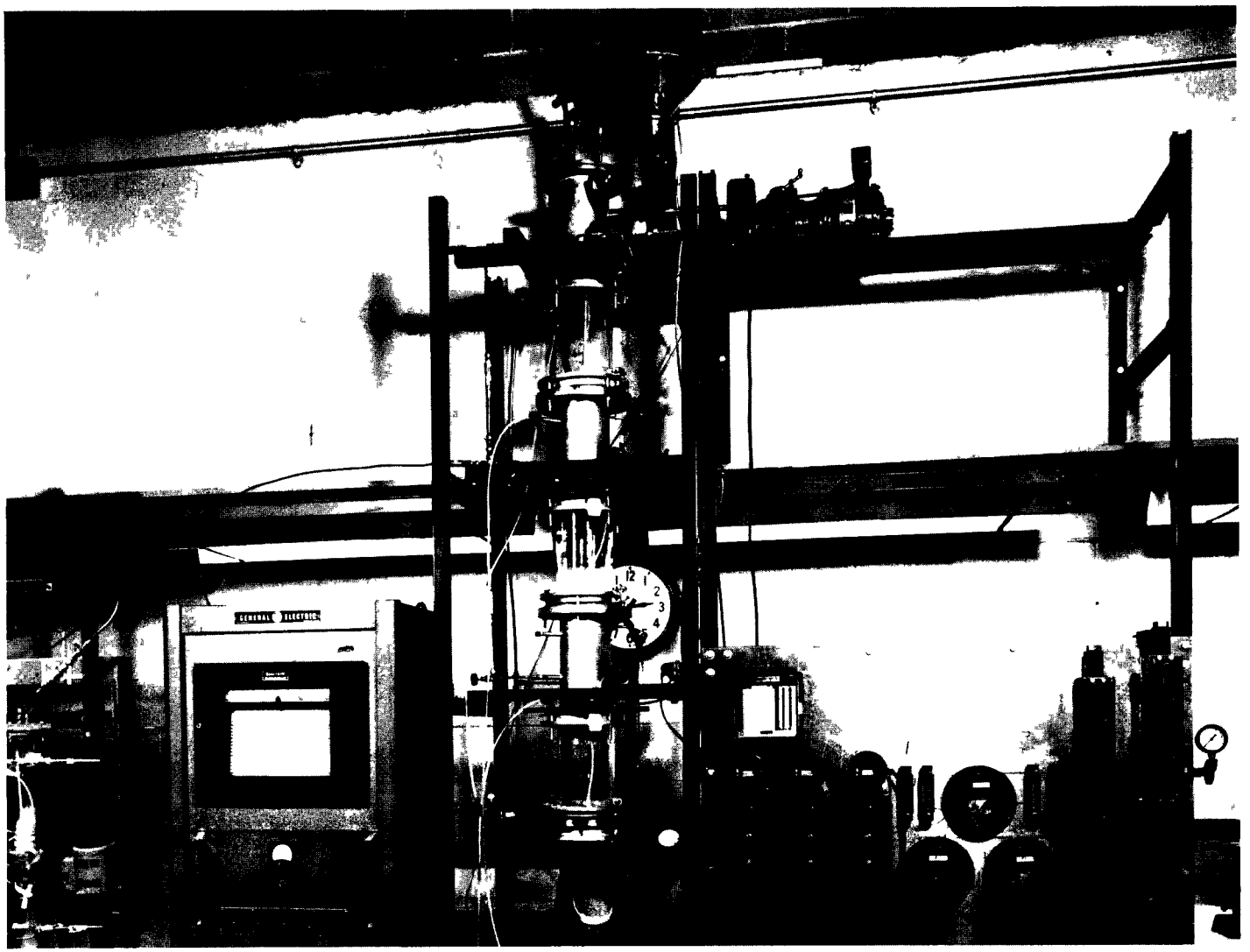

Figure 2. Photograph of the Multistage Fluidization Column and Auxiliary Equipment

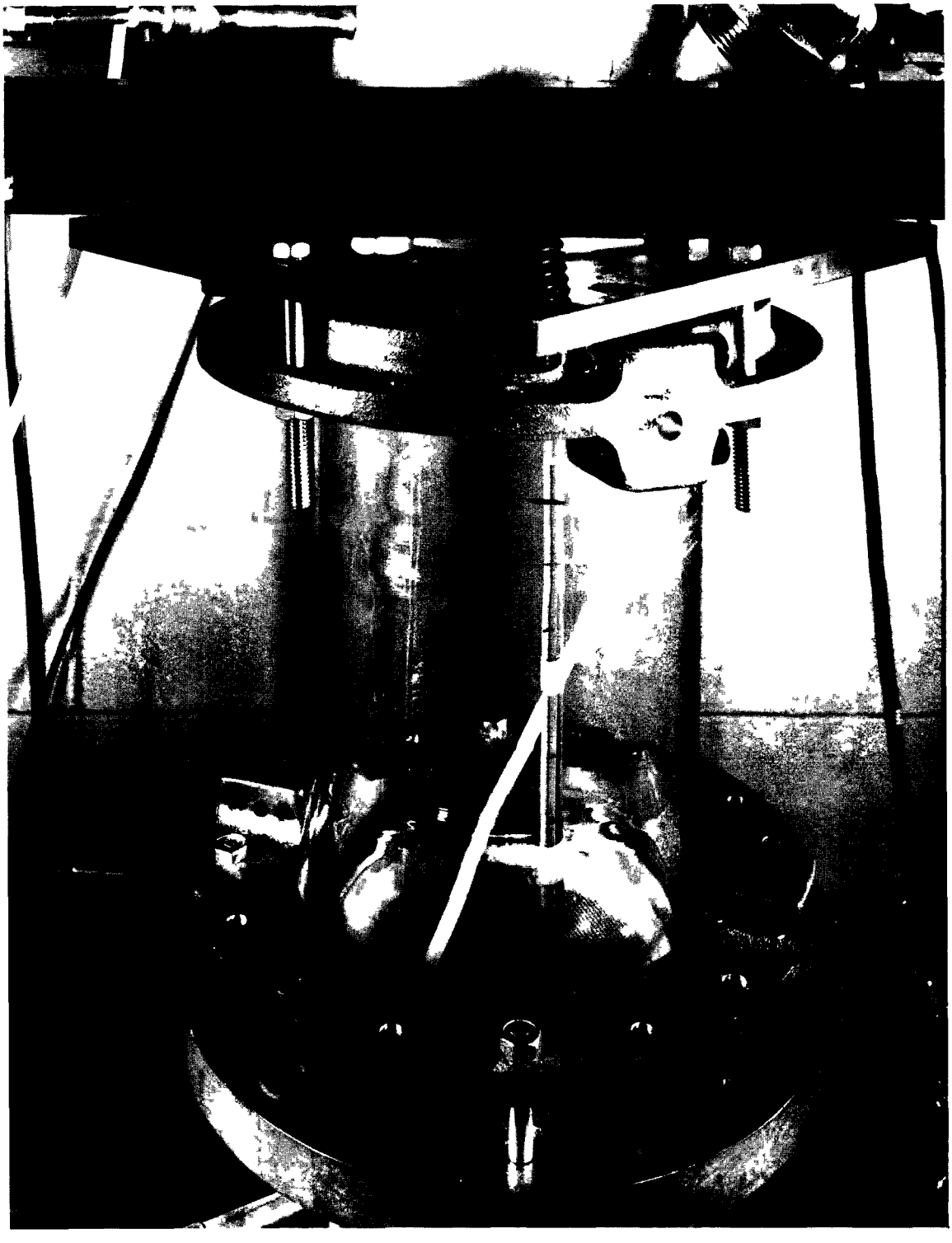

Figure 3. Photograph of a Stage in the Six-inch Column

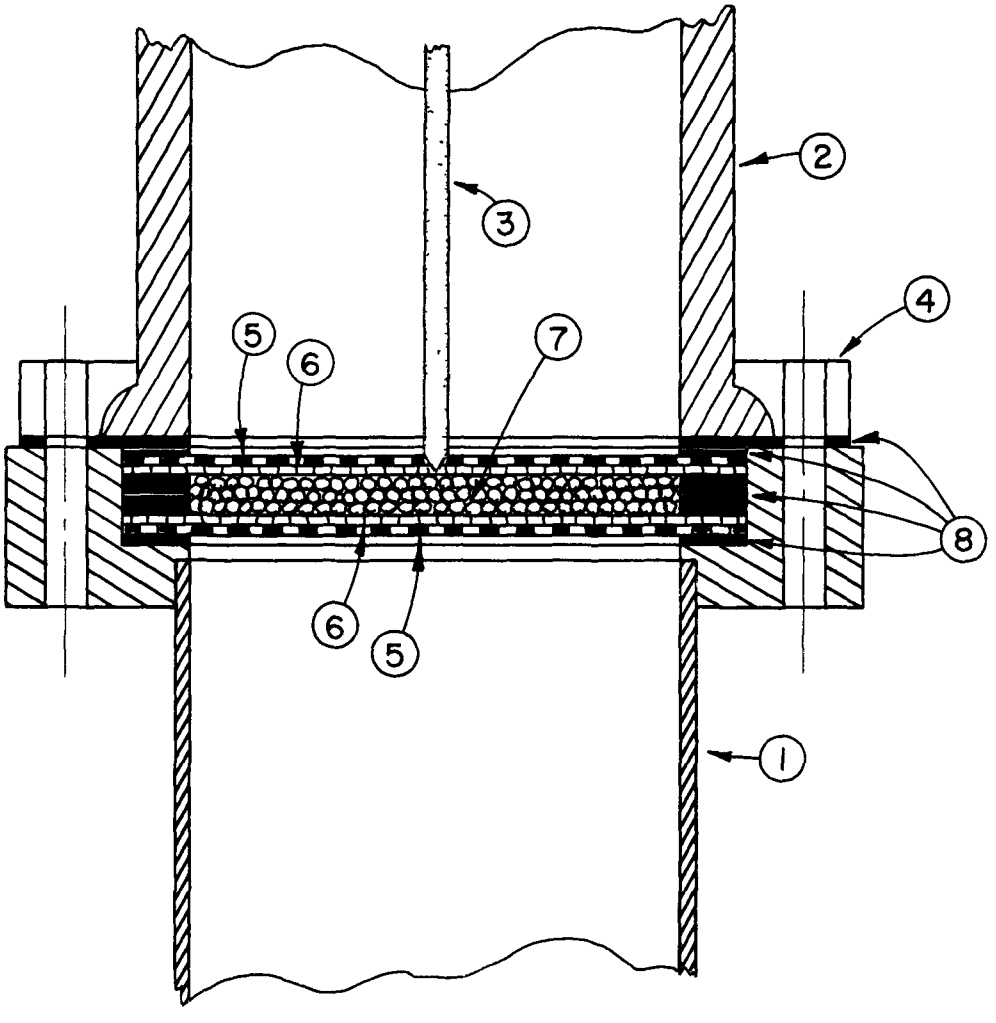

(1) TOP OF BRASS SECTION
(2) BOTTOM OF GLASS SECTION
(3) VIBRATOR-PLATE CONTACTOR
(4) FLANGE
(5) PUNCHED PLATE
(6) WIRE SCREEN
(7) INERT BEADS
(8) RUBBER GASKETS

Figure 4. Schematic Diagram of a Plate in the Multistage Column

from an air-operated vibrator (one for each plate), located outside the column, to the plate by means of a 1/4-inch diameter steel rod. One end of the rod was pointed and fitted into any hole in the plate cover. At the other end of the rod a vibrator was attached. The vibration was thus transmitted along the rod from the vibrator to the plate. The rod entered the column through a rubber stopper that provided the gas seal; diaphragm or bellows seals could be used for the same purpose.

3. Auxiliary Equipment

The bed-level control system depended upon sensing differential pressure across each bed. The pressure was magnified by Taylor pressure transmitters (one for each stage) and recorded by a three-pen Taylor Transcope recorder. Three Mercoid switches, operating on signals from the transmitters, opened and closed electrical circuits to the solenoids located in the air-supply lines of the vibrators.

The fluidizing-gas rate was determined by passing the gas through a rotameter after it had been humidified. The humidification was necessary to eliminate static electricity within the bed.

The humidifier consisted of two 4-inch I.D. stainless tubes each 2-feet long (Figure 5). The first contacted the gas and the water while the second removed any entrained droplets.

For the mass-transfer work a General Electric dew-point recorder was utilized. A schematic for this recorder is shown in Appendix II.

B. Discussion of Column Operation

1. Static Electricity

Part 1 of the experimental work involved the use of glass beads as feed material (See Appendix I for the feed material specifi-

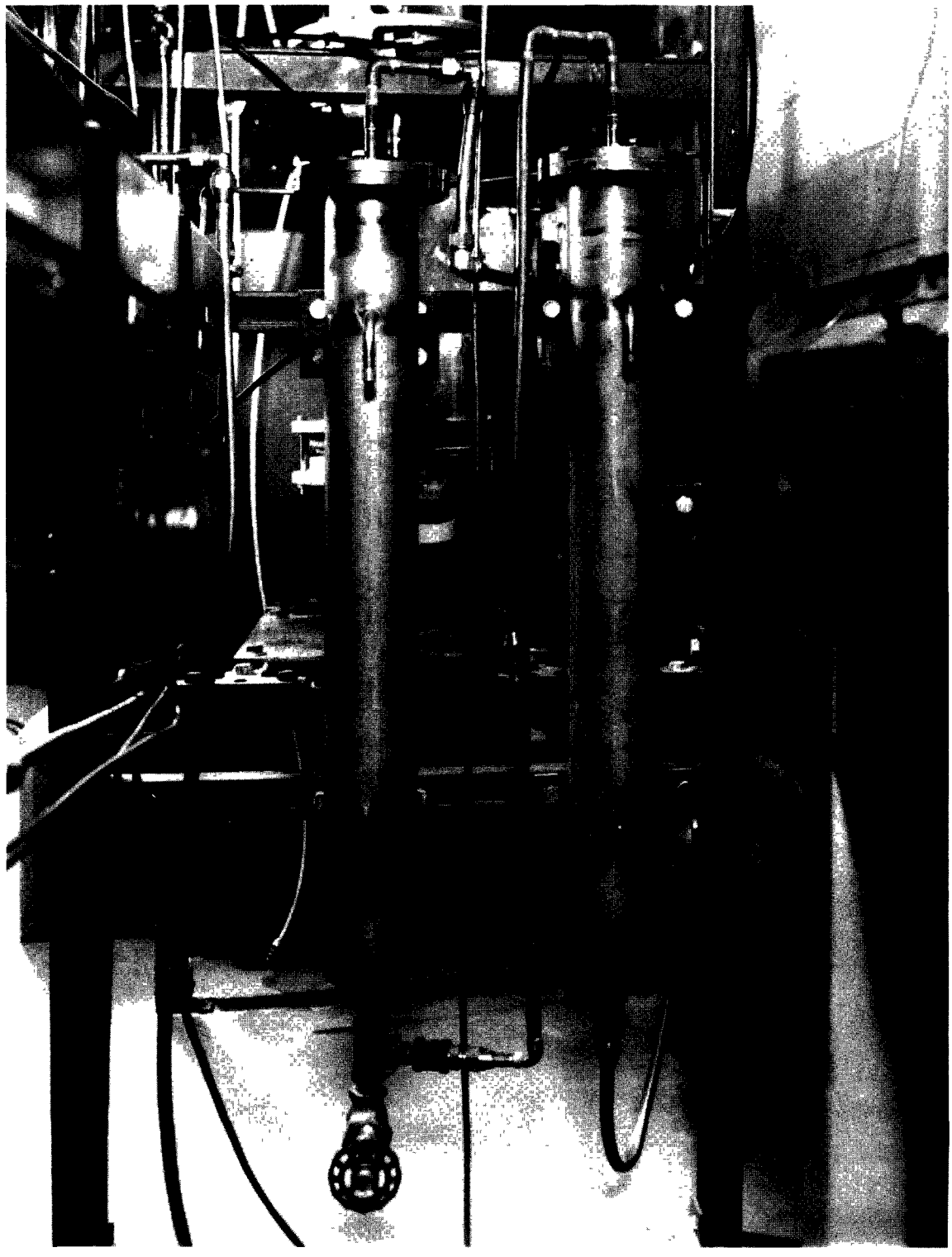

Figure 5. Photograph of the Humidifiers

cations). With dry air (dew point of -80°F) as the fluidizing gas, the glass beads became charged with static electricty. This led to non-reproducible experimental data because the beads agglomerated and stuck to the sides of the glass column. The static electricity was eliminated by fluidizing the bed with air having a dew point of approximately 25°F (28% absolute humidity). It should be noted that saturated fluidizing air caused the bed to cake thus stopping operation of the column completely.

2. Feed Mechanism

At high, fluidizing-air velocities it was necessary to pressurize the feed hopper in order to maintain the desired feed rate. If the pressure in the hopper was considerably higher than that in the top of the column the feed would blow past the screw and the housing of the feeder thus nullifying the ability to control the feed rate by means of the variable speed transmission.

3. Vibrators and Plate Contactors

The efficiency of vibrator operation depended upon how the vibrators were attached to the rod. Vibration was produced by a rotating steel ball that generated centrifugal force as it rotated within the vibrator. It was found that vibrators rigidly attached to an immovable object dissipate the available energy from the expanding air almost entirely as centrifugal force (maximum RPM). The only losses in this case were entrance and exit losses of the air and frictional losses to the vibrator wall by the revolving steel ball. If the vibrator was loosened, additional energy went into motion of the vibrator itself. Under these conditions less energy was available for centrifugal force and the revolving ball slowed down.

Some difficulty was encountered in maintaining a constant vibrational frequency (hence, uniform throughput rates on all three plates) since this depended upon the pressure of the supply air. However, the use of pressure regulators in the air lines kept this difficulty to a minimum.

4. Bed-Level Control

The beds were easily maintained within 1/2 inch of the desired fixed-bed depth. No difficulties were encountered with the Mercoid switches or pressure transmitters. The pressure-tap lines from the column to the transmitters were cleaned frequently to prevent buildup of solids. Occasional clogged lines caused inaccurate differential-pressure readings which resulted in buildup or emptying of the beds involved.

Part 1.

DESIGN STUDY

IV. PART 1 - DESIGN STUDY

This work was done to determine the operational characteristics of a newly designed multistage fluidization column. The distinguishing feature of the equipment was the use of vibration to achieve downward transport of solids from stage to stage through a plate consisting of spherical material "sandwiched" between a cover and support screen. Several variables were studied and the data were then incorporated into a design correlation.

A. Scope

Glass beads were fluidized with air in the six-inch diameter, three-stage column. The throughput rate was determined as a function of (1) vibrator size and vibrational frequency, (2) feed particle size and density, (3) plate resistance, (4) superficial air velocity, (5) fluidized-bed depth, and (6) vibrator on-time. The extent to which the variables were investigated is shown in Table 1.

Table 1

Scope of the Variables Tested

Variable	Range		Max/Min
	Min	Max	
Feed diameter, in.	0.0030	0.0110	3.66
Feed density (bulk), g/cc	0.720	1.5	2.09
Shape factors, dimensionless	1	1.62	1.62
Air velocity, ft/sec	0	0.50	-
Bed depth, in.	3	9	3
Throughput rates, $ft^3/hr\text{-}ft^2$	0	15	-
Vibrator on-time, %	0	100	0
Depth of inert beads, in.	0.072	0.436	6.05
Diameter of inert beads, in.	0.0357	0.118	3.31
Density of inert beads, g/cc	0.720	5.4	7.5

B. Preliminary Work

1. Cover Plate

In the original column constructed at the Pennsylvania State University there was no cover plate incorporated into the bed support and the inert beads could, under the influence of the fluidizing gas, become unevenly distributed. Under these conditions, stable operation of the column was limited to superficial air velocities no higher than twice that required for minimum fluidization. At higher velocities the increased motion of the fluidized bed dug holes in the layer of inert beads thus lowering the plate resistance and causing very large uncontrolled throughput rates. Preliminary work at Argonne, in a two-inch glass column, using the glass-bead air system, showed that the use of a cover plate (pressing on the inert beads) eliminated this problem, thus making stable column operation possible over a much wider gas velocity range (up to ten times the minimum velocity for fluidization--the experimental maximum).

2. Internal Vibrators

A major improvement over The Pennsylvania State University column resulted from the use of "internal" vibration. When vibration was applied on the outside of the column, as was done previously, throughput occurred on all plates. Such throughput was nonreproducible. Some means was necessary to damp the vibration between plates. It was found that this could be accomplished by transmitting the vibration from outside the column directly to each plate by means of a metal rod. This transmitter simply conducted the vibrations from the vibrator to the plate. A flexible seal such as a

bellows or rubber stopper was necessary where the transmitter entered the column in order to eliminate transmission of the vibration to the column itself. Under these conditions the throughput was selective, occurring only on the plate vibrated.

3. Level Control

The method used to control the bed level on each plate of the six-inch column resulted from the use of internal vibration. Since throughput occurred only on the plate vibrated, the on-off cycle was determined in the following manner. The differential pressure (one to twelve inches of water) across each plate was sensed and magnified to from 3 to 15 psig by a Taylor differential-pressure transmitter. The outputs of the transmitters were fed to Mercoid differential pressure controllers and to a Taylor three-pen Transcope recorder. The latter made a permanent record of the differential pressure across each of the three stages during the experimental work. The Mercoid pressure controllers controlled electrical circuits to solenoid valves in the vibrator air lines. The pressure switches were set to open and close at the desired differential pressures. A minimum change of 1/2 psig in differential pressure was required. When the higher set-pressure was reached the circuit to the solenoid was closed thus turning on the air supply to the vibrator. With the vibrator in operation bed material passed downward through the support plate to the plate below. The loss of material on the plate caused the differential pressure to decrease. When the value of the differential pressure had reached the lower set-point value, the circuit to the solenoid was opened, and the air supply to the vibrator stopped thus halting the downward transport of solids.

The frequency of the on-off cycle depended upon the feed rate. For given operational conditions the maximum throughput rate occurred with the vibrators in operation 100 percent of the time. A linear relationship was found to exist between the throughput rate and the percentage of time that the vibrators were in operation.

C. Procedure

Each of the three beds was initially filled to the desired depth with feed material. This was accomplished by feeding in material on the top plate and operating the vibrators on the two upper plates until the bottom stage was filled. Then the middle-stage vibrator was turned off to fill this stage. With this accomplished, the top plate was filled to the desired depth. The feed hopper was then loaded and the screw-feeder drive set to the operating feed rate. The fluidizing air was then turned on with the rate regulated by a valve located at the inlet to the air rotameter. The running time indicator was set to zero. The electrical circuits to the Mercoid switches, the screw-feeder drive and the running-time indicator were then simultaneously closed.

The product collected in the bottom of the column throughout the run. It was then released into a small, weighed cardboard drum by opening a 1/2-inch gate valve located at the extreme bottom of the column. The product was then weighed and the throughput rate determined. The runs varied from 2 to 30 minutes depending upon the throughput rate. The percentage of the total run time that the vibrators were in operation (hereafter referred to as vibrator on-time) was determined from electrical timers located in the solenoid air-vibrator circuits and from the total length of the run. These timers registered the total

time that the air vibrator circuits were energized.

In all runs, the raw data were plotted as vibrator on-time versus throughput rate with the parameters being the variables under study.

The corrections applied to the rotameter readings to determine superficial air velocities in the column are described in Appendix I.

Each of the vibrators was adjusted to give the same vibrational frequency for any given run. This frequency was checked for consistency throughout the runs. If the vibrator on-time differed more than 10 percent between plates, the run was discarded. In all calculations, the average vibrator on-time for the three plates was used. Water was periodically added to the humidifier in order to ensure static-free operation of the column.

D. Discussion of the Experimental Results

At the beginning of the following sections, D-1 through D-6, a table is presented showing the operating conditions for the study. Additional information, including the experimental data are included in Appendix I.

1. Vibrational Frequency

In Table 2 the operating conditions for this study are tabulated.

Model BD, Martin Engineering Co. (Neponset, Illinois), air vibrators of two sizes--No. 10 and No. 13--were used in this work (Figures 8 and 11). Throughput rates as a function of vibrator on-time were determined for various vibrational frequencies from 6000 to 10000 CPM. The vibrational frequencies were determined by direct reading of a Fowler Vibra-Tak--a reed-type vibration indicator.

Table 2

Operational Conditions for Vibrational Frequency Study

Cover and support plate	40 mesh screen, 13 mesh punched plate
Contactor	No. 300 (See D-2)
Diameter of glass feed particles, D_p	0.0039 in. (No. 130)
Bed depth, H	7 in.
Superficial air velocity, u	0.19 ft/sec
Depth of inert beads, L	0.218 in.
*Vibrator	BD-10 and BD-13
*Vibrational frequency, S	6000 to 10000 CPM
Run numbers	I224-243
Diameter of inert beads, D_I	0.0357 in. (glass)

* Variables for this study

The experimental data from runs using No. 10 vibrators on each plate are shown in Figure 6. The results from No. 13 vibrators are shown in Figure 7. As seen in these figures, the maximum throughput rates (vibrator on-time equal to 100%) in all cases increased as the vibrational frequency increased.

In the air vibrators centrifugal force is generated by a revolving steel ball. This centrifugal force is a function of the physical properties of the vibrator and the vibrational frequency. It can be calculated from the following equation in which F_c is the centrifugal force (lb), W the ball weight (lb), R the radius of rotation (in.), and S the vibrational frequency (CPM).

$$F_c = 0.0000284\ WRS^2 \qquad (1)$$

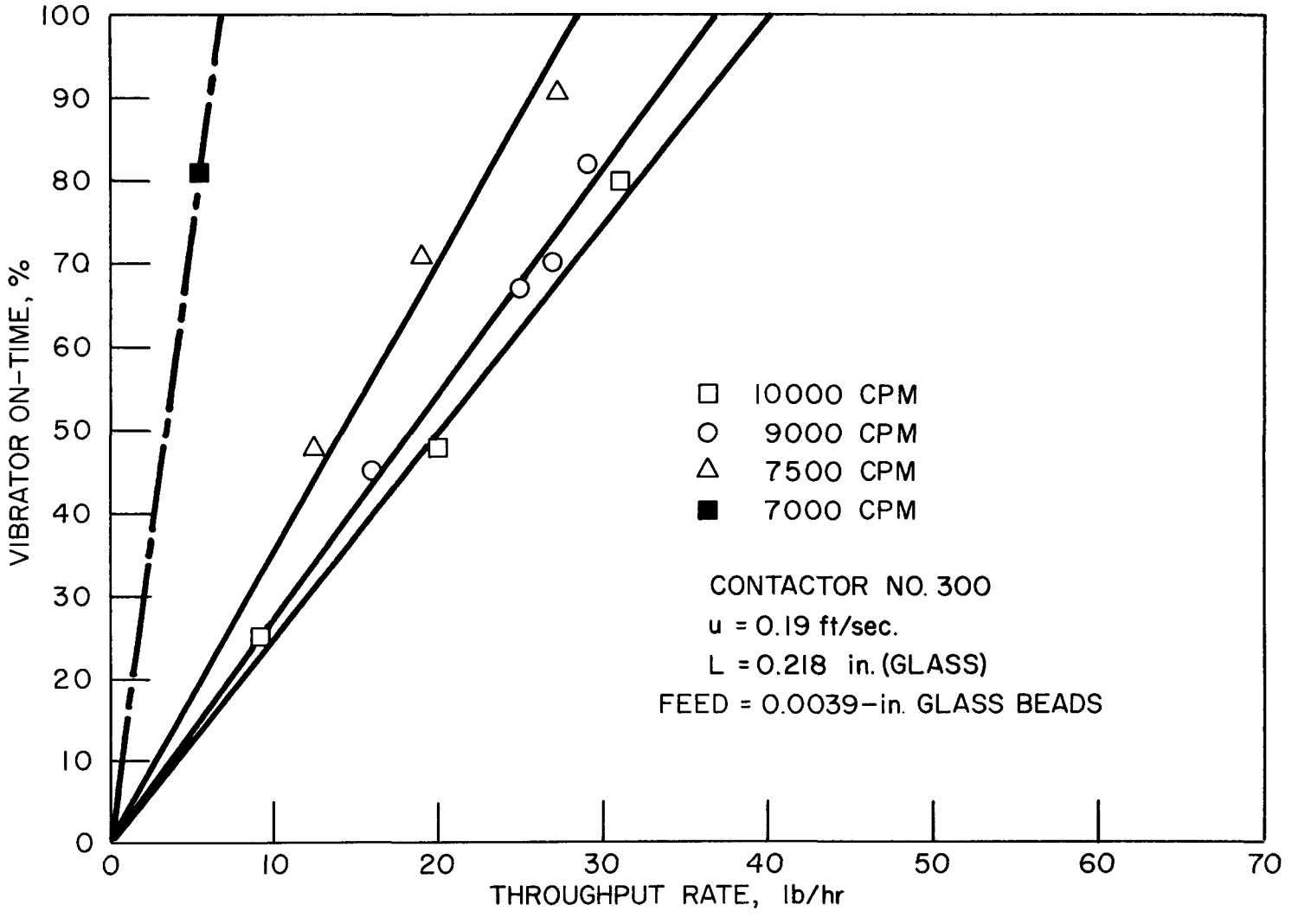

Figure 6. Vibrator On-time vs Throughput Rate for No. 10 Vibrators

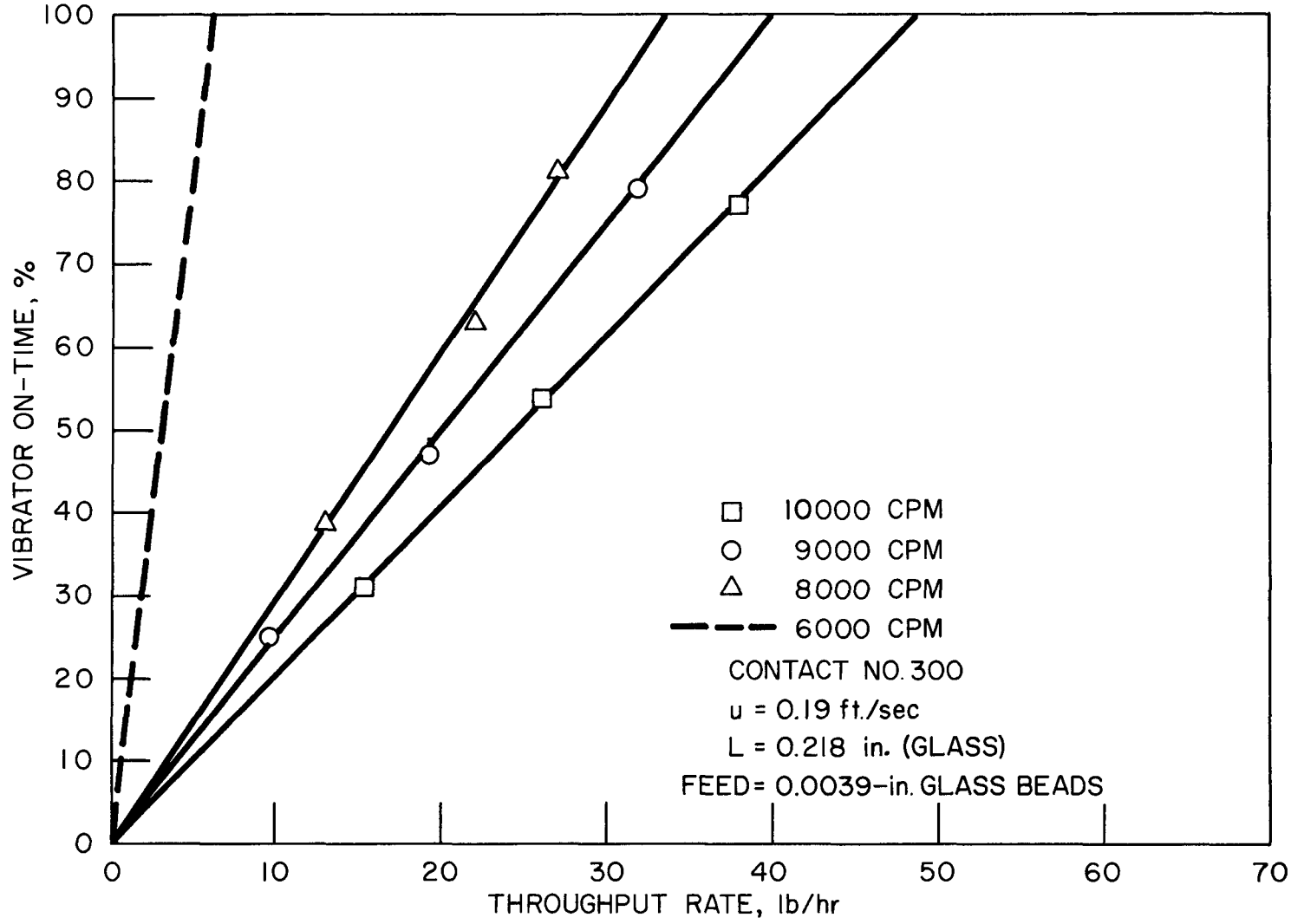

Figure 7. Vibrator On-time vs Throughput Rate for No. 13 Vibrators

This equation is derived in Appendix I. The physical properties of the vibrators along with a schematic diagram are shown in Figure 8.

A plot of centrifugal force versus maximum throughput rate (Figure 9) with vibrator on-time as a parameter does not correlate the data from both vibrators into a single set of curves. However, when two correction factors are applied to the centrifugal force making it, in effect, an energy per unit-vibrator-weight term, the data from both vibrators falls on one set of curves (Figure 10). The correction factors are lever arm length (See Figure 8) and total vibrator weight. The centrifugal force is multiplied by the lever arm length because it acts to magnify the generated force and is divided by the total vibrator weight since a heavy vibrator absorbs more energy then a light one. Thus in a heavy vibrator a smaller percentage of the generated energy is available for transmission to the plate.

Number 10 vibrators at 8000 CPM were used for the design experiments. In the design correlation (Part V) the effect of vibrational frequency is not included.

2. Contactors

After completion of the vibrational-frequency study the efficiency of several contactors was investigated. A photograph of those tested along with their code numbers is shown in Figure 11. The operating conditions for these runs are shown in Table 3.

For a basis to calculate the efficiency of the various contactors, contactor No. 300 was arbitrarily chosen to be 100% efficient. This choice was made because of the data obtained on this contactor in the vibrational frequency studies. Contactor No. 300

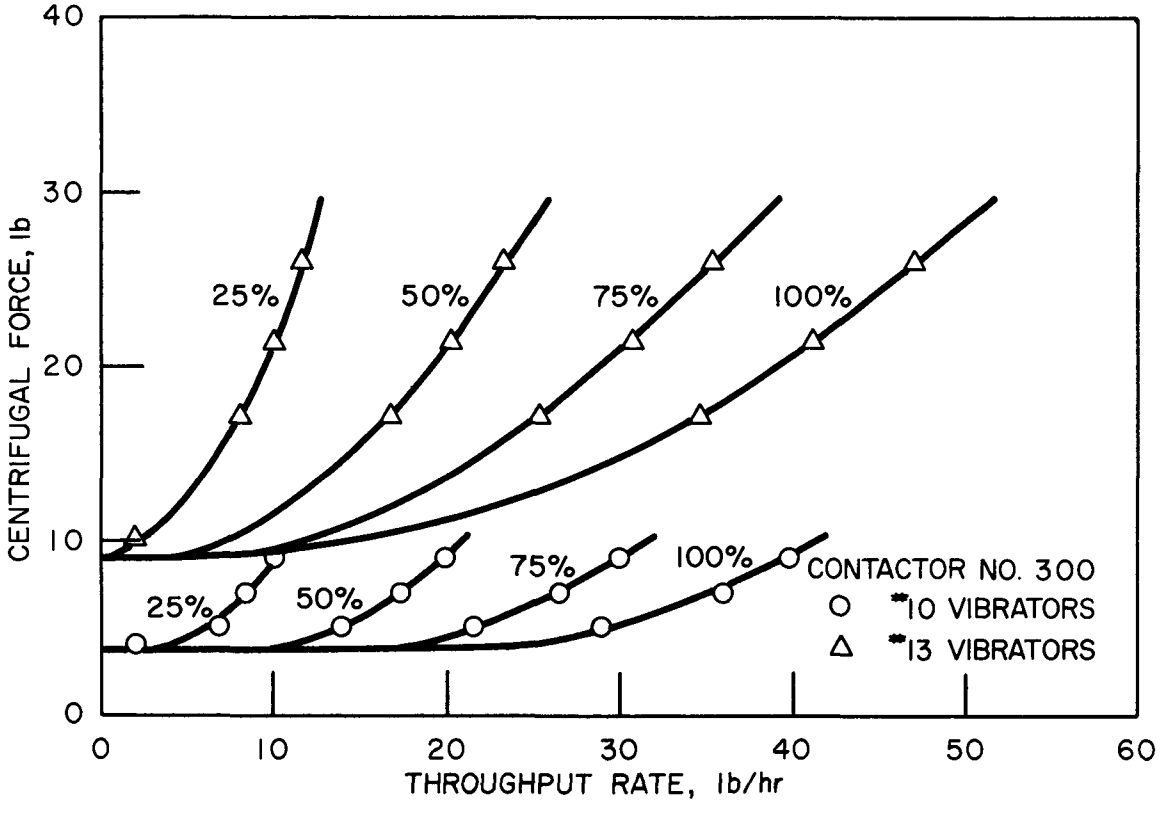

Figure 9. Centrifugal Force vs Throughput Rate with Vibrator On-time as the Parameter

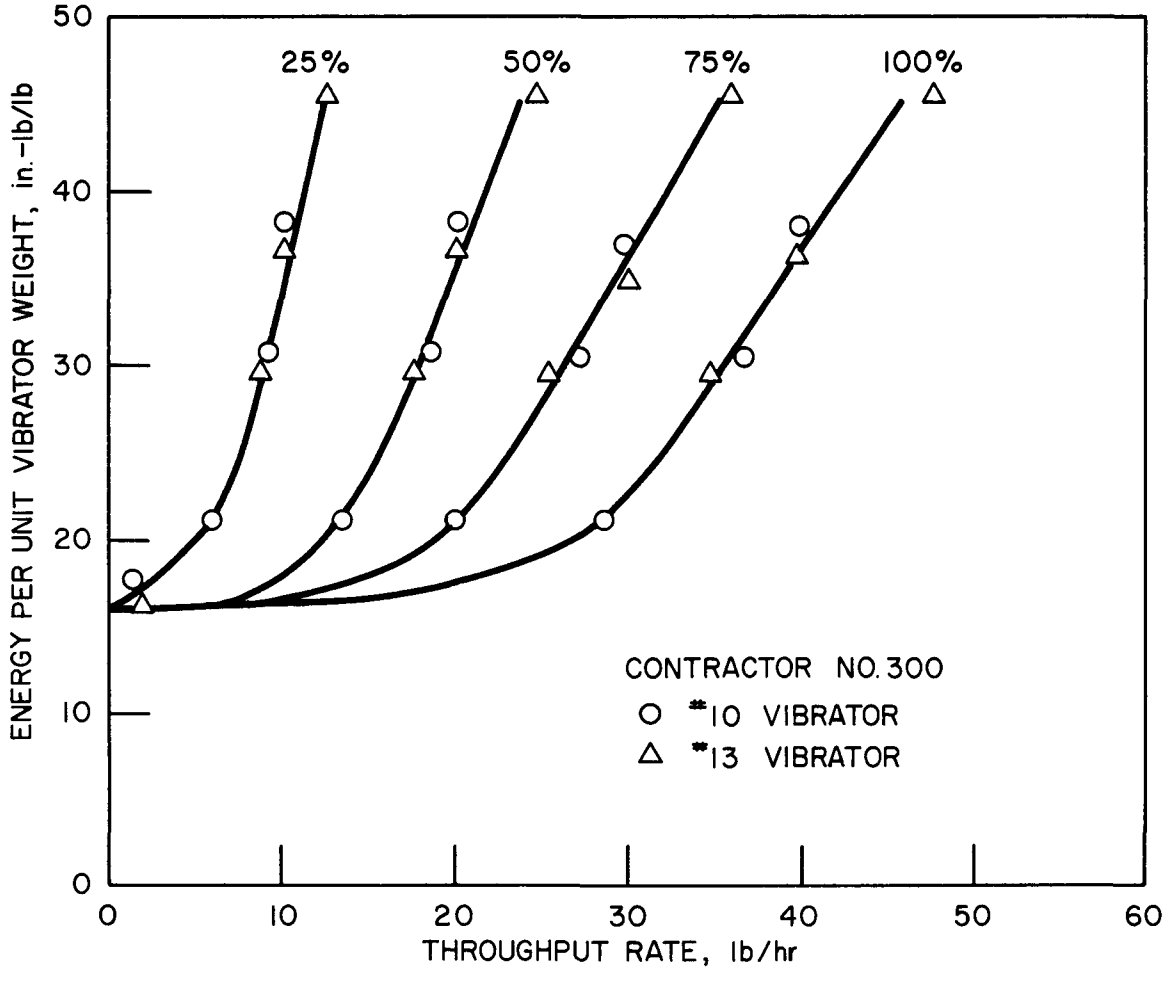

Figure 10. Energy per Unit Vibrator Weight vs Throughput Rate with Vibrator On-time as the Parameter

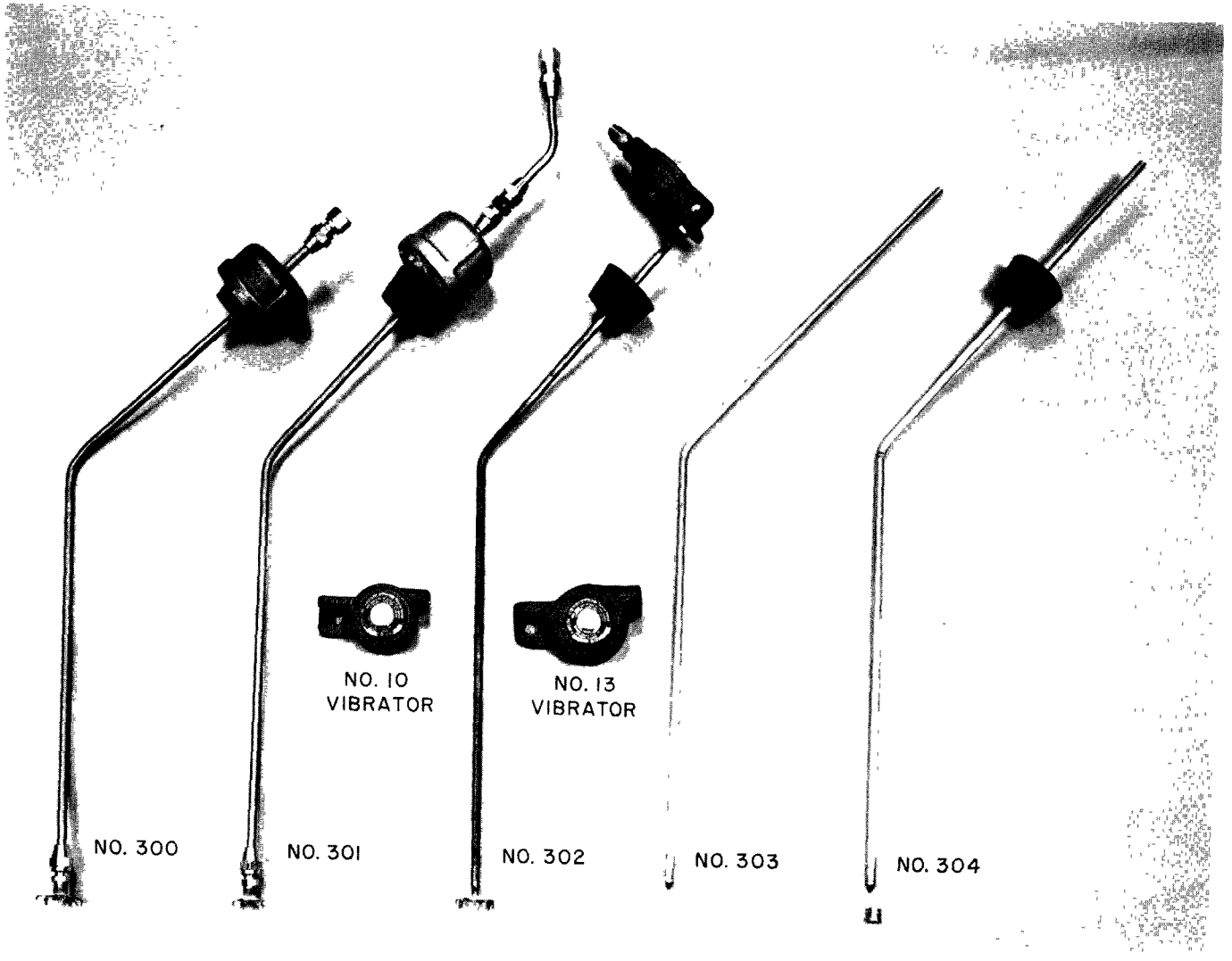

Figure 11. Photograph of the Vibrators and Contactors

consisted of a hard copper tube with the vibrator located at one end. A copper claw was attached to the other end of the tube by means of a flare fitting. The prongs of the copper claw were forced into the holes of the cover plate, thus completing the transmission line from the vibrator to the plate.

Table 3

Operational Conditions for Contactor Study

Cover and support plate	40 mesh screen, 13 mesh punched plate
*Contactors	#300, 301, 302, 303, 304
Diameter of glass feed particles, D_p	0.0039 in. (No. 130)
Bed depth, H	7 in.
Superficial air velocity, u	0.19 ft/sec
Depth of inert beads, L	0.218 in.
Vibrator	BD-10 and BD-13
*Vibrational frequency, S	7500 to 11000 CPM
Run numbers	I300-308, I220-233
Diameter of inert beads, D_I	0.0357 in. (glass)

* Variables for this study

The efficiency for each of the investigated contactors was determined with the aid of Figure 10. For each contactor tested, runs were made at a constant energy-per-unit-vibrator-weight (ordinate of Figure 10). From the experimental data the throughput rates for vibrator on-times of 25%, 50%, 75%, and 100% were determined. The efficiency was then evaluated from the following equation for each

of the vibrator on-times. These were then averaged to get the reported efficiencies for each contactor.

$$E_c = \frac{\text{Ordinate Fig. 10 for contactor No. 300 at throughput rate of new contactor}}{\text{Energy per unit vibrator weight used in study of new contactor}}(100) \qquad (2)$$

Figure 12 presents the experimental data as a plot for vibrator on-time versus the throughput rate for the contactors studies. The efficiencies of each are summarized in Table 4.

Table 4

Contactor Efficiencies

Contactor No.	Average Efficiencies
300	100%
301	42%
302	147%
303	225%
304	203%

Contactor No. 301 was identical to No. 300 except for the addition of a short piece of soft copper tubing which permitted mounting of the vibrator in a horizontal position (See Figure 11). The low efficiency of 42% is attributed to high energy losses in the flare connection between the original copper tubing and the additional piece.

The solid-steel-rod contactor (No. 302) gave an efficiency of 147%. This was attributed to better energy transmission in the relatively unyielding steel rod as compared to the copper tubing

contactors. In this contactor, contact with the plates was made by a copper claw identical to that used in contactors No. 300 and 301. However, the claw was soldered to the rod in this case.

The highest efficiency (225%) was attained with the simplest contactor (No. 303). This contactor consisted of 1/4-in. diameter solid steel rod one end of which was machined to a 330° point. This point fitted tightly into any hole in the cover plate. The high efficiency is attributed to its simple design and consequent absence of areas for energy losses. Because of its high efficiency, simplicity, and durability this type of contactor was used for all of the remaining design studies. After approximately 75 hours of operation, the points and the holes in which they were placed were examined for wear. Slight wear had occurred on the points in the form of a "seating" ring the diameter of the plate hole. This is illustrated in Figure 13.

Contactor No. 304 gave a high efficiency of 203% and was relatively complex in construction. It consisted of a 1/4-in. diameter brass rod with a 300° pointed end. Instead of fitting into the cover plate, the pointed end was placed into a machined fitting which had been previously soldered to the cover plate (see Figure 11). Difficulty was encountered in seating the point properly.

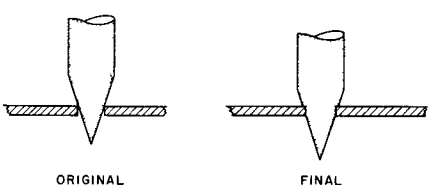

Figure 13. Contactor No. 303 Point Wear

With a corrosive system or a process involving high temperatures it would not be possible to use a rubber stopper for the column-contactor seal. A corrosion-resistant seal was developed and is shown schematically in Figure 14. The use of swagelock fitting

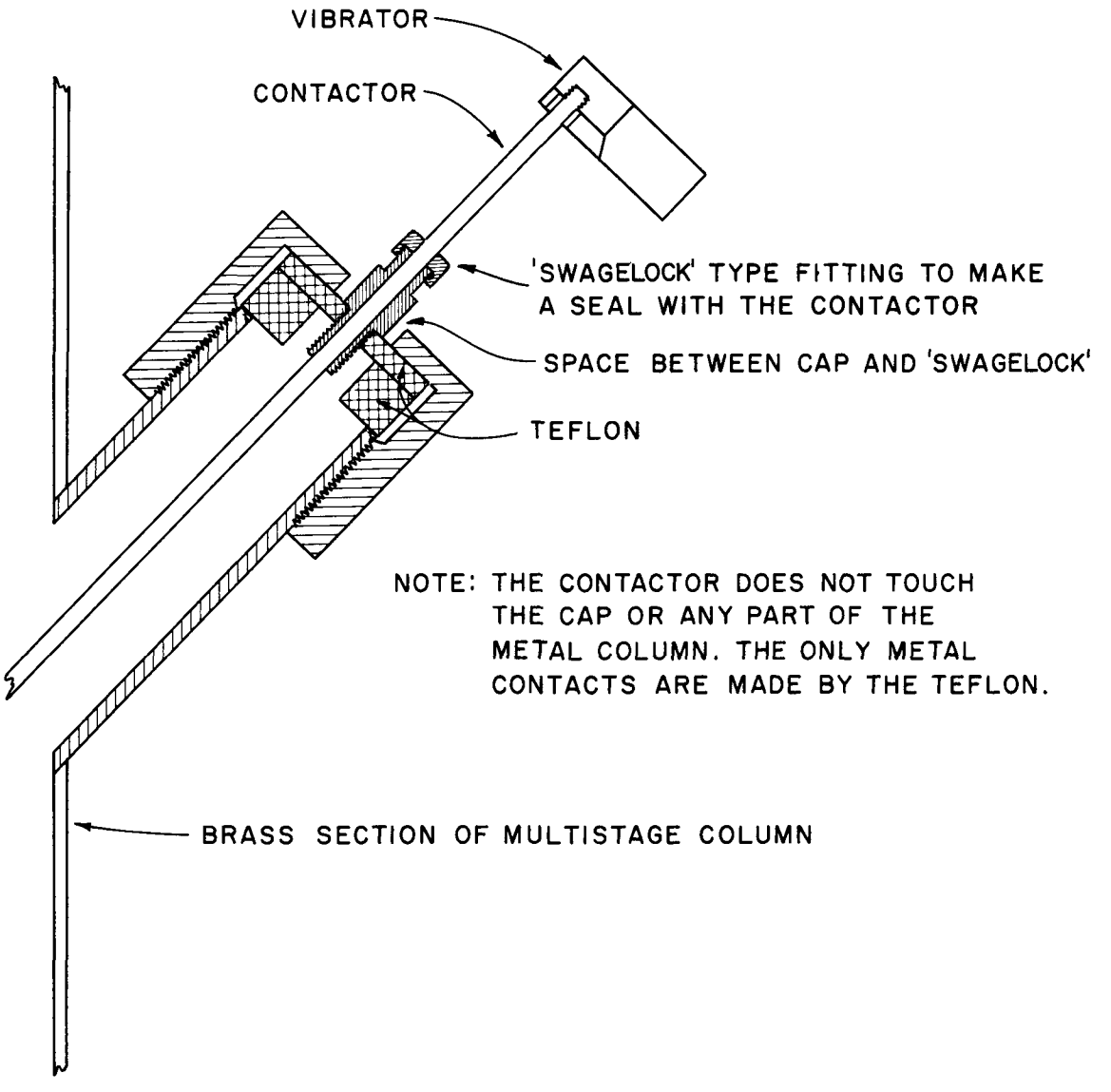

Figure 14. Schematic Diagram of Corrosion-resistant Seal

and teflon spacers for the seating material gives the necessary resistance to corrosive and high temperature operation. To maintain high contactor efficiency it was found necessary to mount the teflon-swagelock combination in such a manner that resiliency was incorporated into the design. A corrosion-resistant metal bellows would provide the same effect. Direct contact to the column itself except through the resilient teflon or bellows seal cannot occur if high efficiency is to be maintained.

3. Feed Particle Size

The operational conditions for this study are presented in Table 5.

Table 5

Operational Conditions for Particle Size Study

Cover and support plate	40 mesh screen, 13 mesh punched plate
Contactor	No. 303
*Diameter of glass feed particles, D_p	0.0045 to 0.0030 in. (No. 120, 130, 140, 150)
Bed depth, H	7 in.
Superficial air velocity, u	0.19 ft/sec
Depth of inert beads, L	0.218 in.
Vibrator	BD-10
Vibrational frequency, S	8000 CPM
Run numbers	1400-406, 1303-305
Diameter of inert beads, D_I	0.0357 in. (glass)

* Variable for this study

The experimental results have been plotted in Figure 15 as vibrator on-time versus the throughput rate. As seen in Figure 15 the maximum throughput rate was achieved with the smallest diameter (0.0030-in.) feed material. From this work the size of the openings in the support and cover plates was found to have little effect upon the throughput rate, as long as the openings were nearly equal in diameter to the inert beads. It was necessary for these openings to be slightly smaller than the inert bead diameter in order to prevent their escape.

Investigation of the data showed that the important factor in controlling the magnitude of the throughput rate is a so-called "critical diameter". This is related to the size of the inert beads and can be defined in the following manner: The "critical diameter" is the diameter of the largest sphere that will pass through the void space between the tightly packed inert beads. The "critical diameter", D_c, is related to the inert bead diameter by the following equation:

$$D_c = D_I/6.46 \qquad (3)$$

This equation is derived in Appendix I. When the difference between the "critical diameter" and the average feed diameter is plotted against the maximum throughput rate (that rate occurring with the vibrator on-time equal to 100%) a straight line results. This is shown in Figure 16. Extrapolation of this line to zero throughput rate shows that a diameter difference, D_c-D_I, greater than 0.0002 in. is necessary for downward transport of solids to occur in a column operating under stable conditions. With unstable operating conditions,

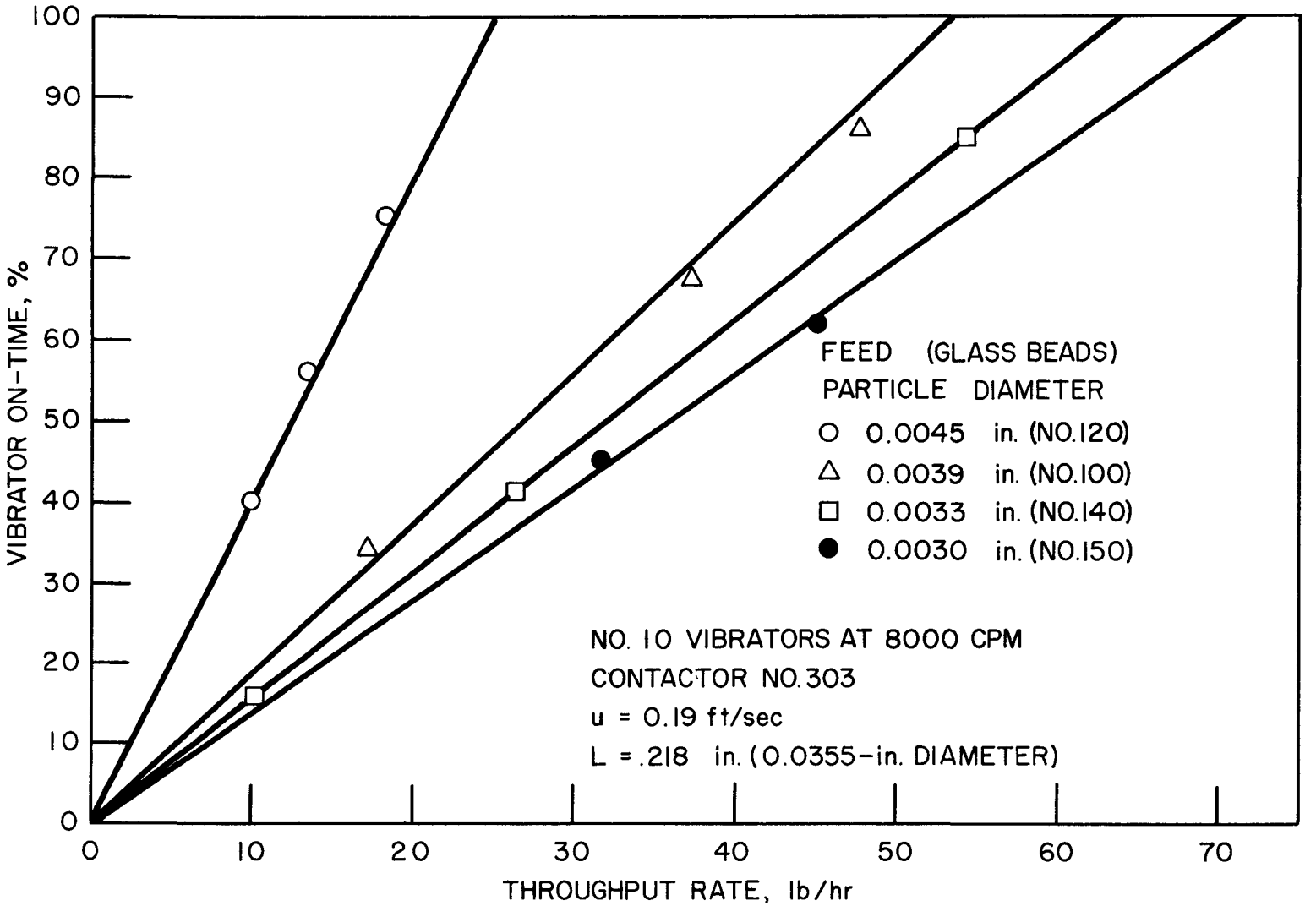

Figure 15. Vibrator On-time vs Throughput Rate for Various Sizes of Glass Feed Material

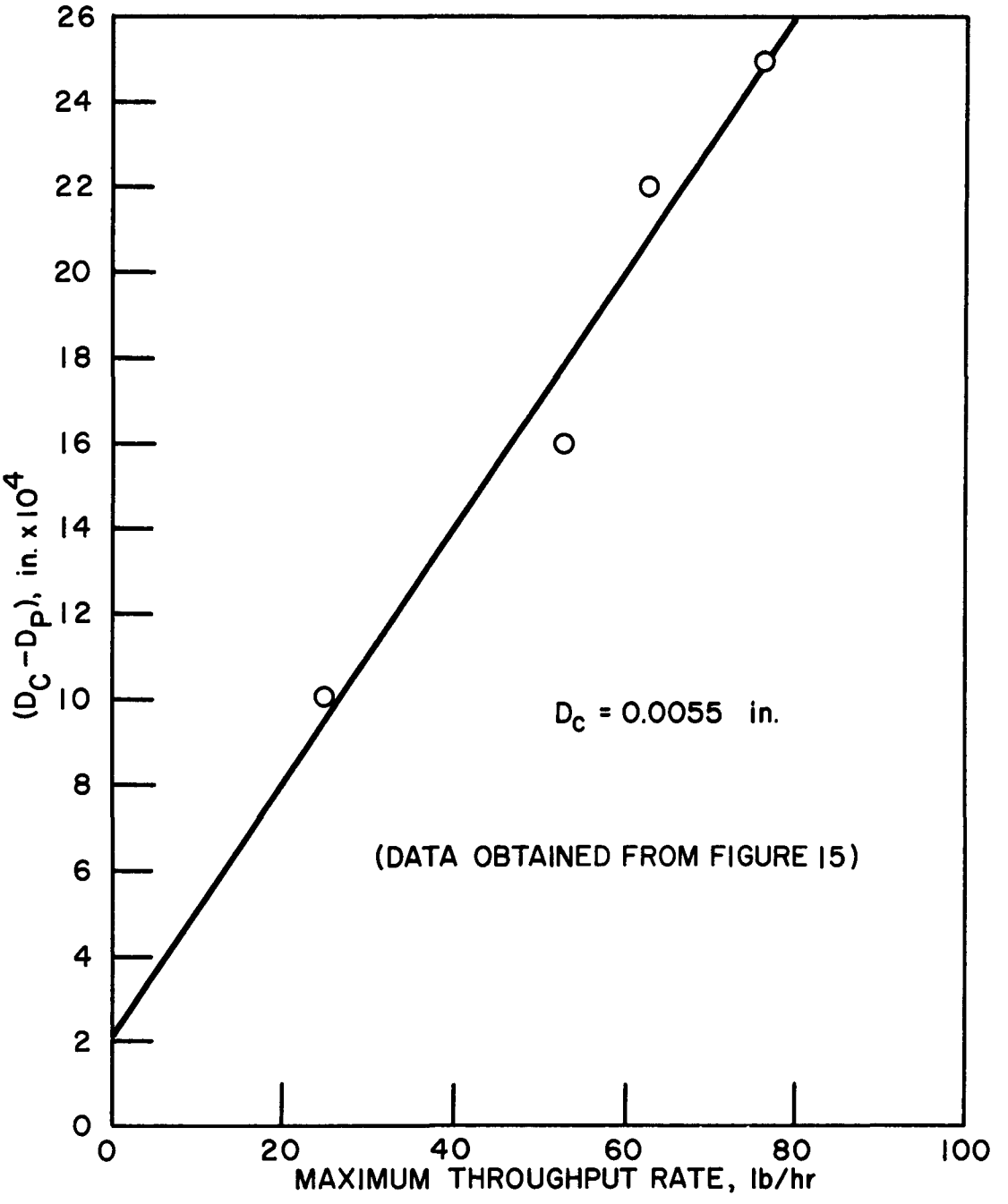

Figure 16. Difference Between Feed Diameter and Critical Diameter vs Maximum Throughput rate

due to very small depths of inert beads, the minimum diameter difference can be negative.

4. Plate Resistance

The plate resistance investigation involved the study of several factors. These will be discussed in the following order: (a) the depth of inert beads on each plate, (b) the density of inert beads and (c) the diameter of inert beads. A summary of the operating conditions for this work is presented in Table 6.

Table 6

Operational Conditions for the Plate Resistance Study

Cover and support plate	40 and 16 mesh screens, 13 mesh punched plate
Contactor	No. 303
Diameter of glass feed particles, D_p	0.0110 to 0.0030 in. (No. 090, 100, 110, 120, 130, 140, 150, 500)
Bed depth, H	7 in.
Superficial air velocity, u	most runs 0.19 ft/sec; some, depending on particle size at 0.21, 0.35 and 0.38 ft/sec
*Depth of inert beads, L	0.072, 0.144, 0.218 and 0.436 in.
Vibrator	BD-10
Vibrational frequency, S	8000 CPM
Run numbers	I500-550, I303-305
*Diameter of inert beads, D_I	0.0357, 0.0592, 0.118 in.
*Inert bead material	glass, activated alumina and copper

* Variables for this study

(a) Depth of Inert Beads on Each Plate

In this phase of the plate resistance work glass beads were used for both the feed and the inert bead material. Throughput rates were investigated at inert bead depths of 0.072, 0.144 and 0.218 inches for feed bead numbers 110, 120, 130, 140, and 150. A superficial vapor velocity of 0.19 ft/sec was used throughout. The experimental data are presented in Figures 15, 17 and 18. From these figures it can be seen that the maximum throughput rate increases for any given feed size as the depth of inert beads is decreased. The dependence of throughput rate, however, is not linear with the depth of inert beads.

From the experimental results discussed above, we can gain an insight into the mechanism responsible for throughput in addition to the "critical diameter" factor. Let us assume that the vibration transmitted to the plates does not impart any motion to the inert beads but does impart sufficient energy to the feed material to insure no clogging of the solids as they pass downward through the plates. With these assumptions and the fact that the free area (cross-sectional) in the plates will determine the amount of material that can pass through the plates we can derive the mimimum theoretical line shown in Figure 19. This was done in the following manner: Experimentally the maximum throughput rate for No. 130 feed beads through a plate having no inert beads and 40-mesh cover and support screens was found to be 360 lb/hr. For this determination, the No. 10 vibrators were operated at 8000 CPM. Under these conditions the free area was 0.059 ft^2. When one layer of inert beads is added to the plate the free area is reduced to 0.042 ft^2 and, assuming a linear

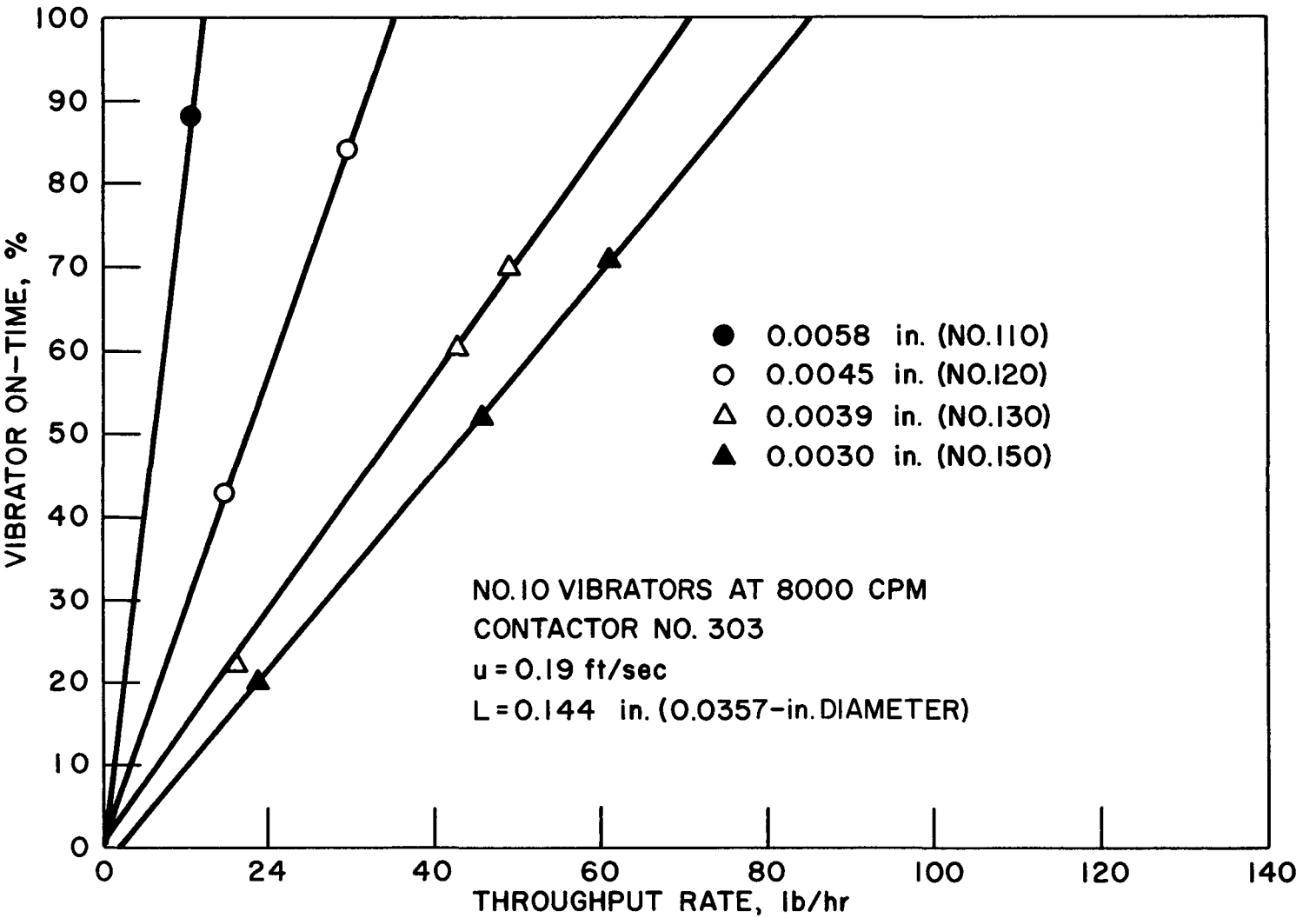

Figure 17. Vibrator On-time vs Throughput Rate with 0.144-in. Depth of Inert Beads

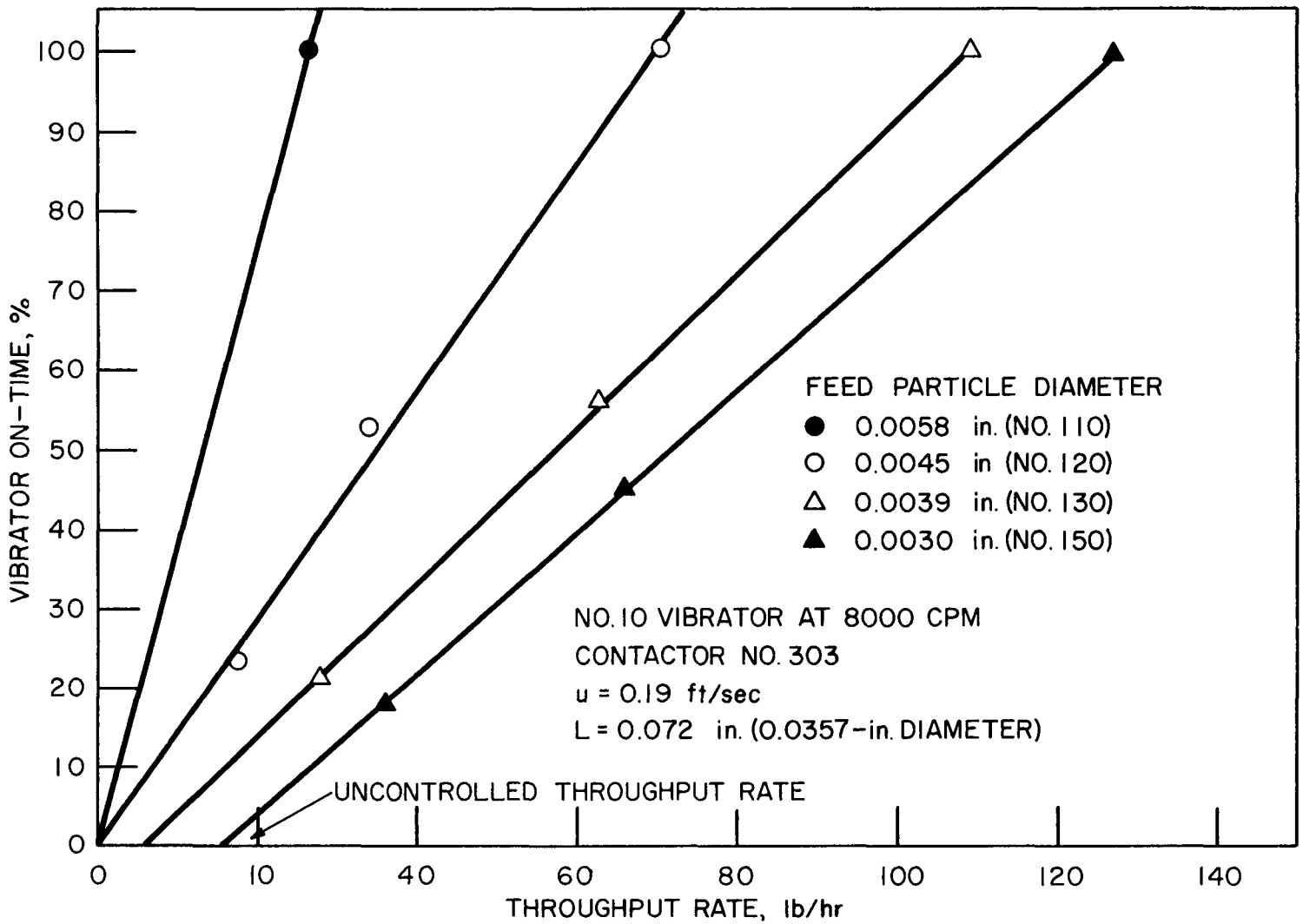

Figure 18. Vibrator On-time vs Throughput Rate with 0.072-in. Depth of Inert Beads

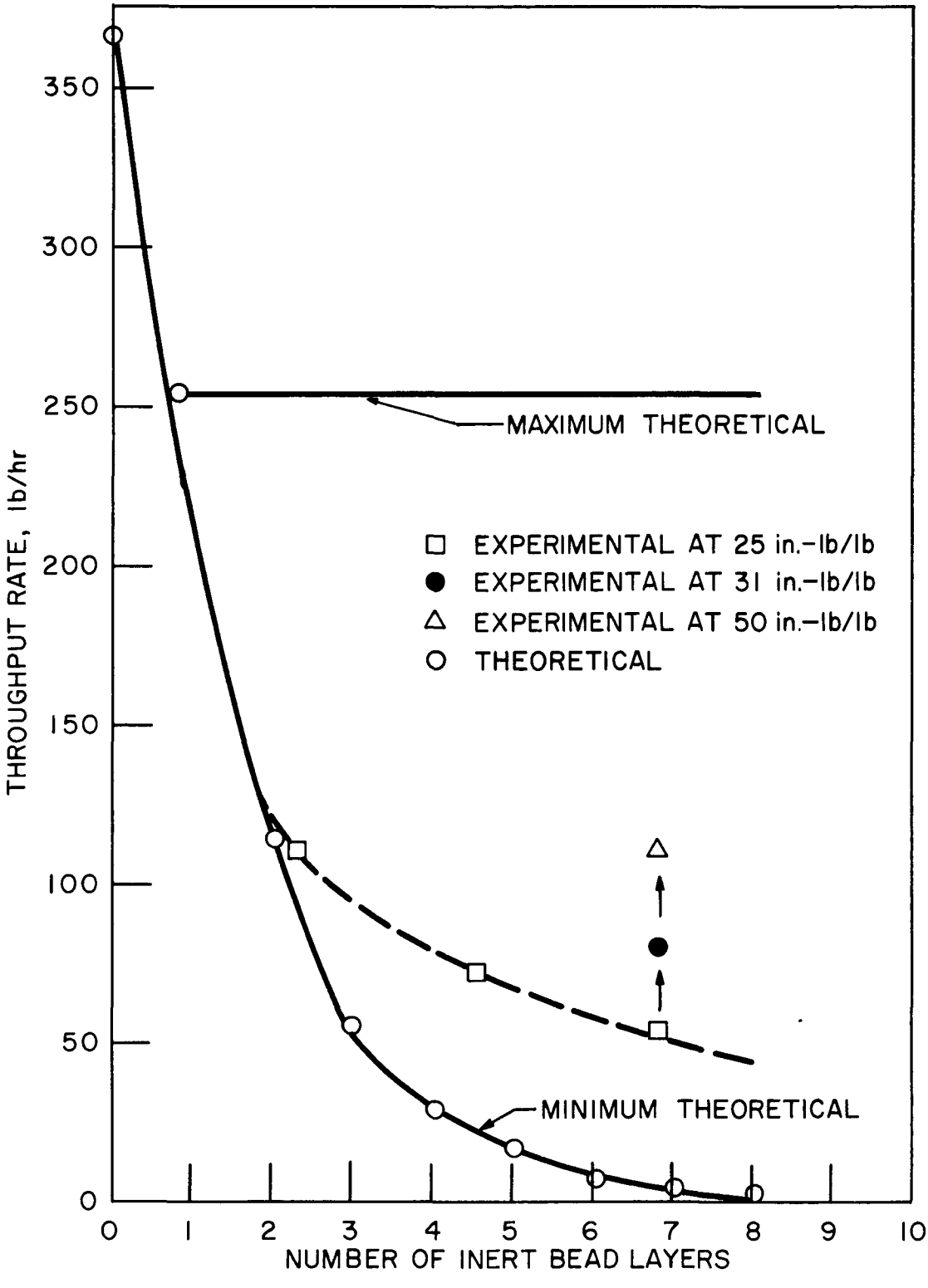

Figure 19. Throughput Rate vs the Number of Inert Bead Layers

(b) Density of Inert Beads

In this investigation copper and activated alumina beads were used as the inert material. Number 120 and 130 glass beads were used as the feed and the results compared with those in which glass beads were used as the inert material. The diameter of the alumina and copper spheres was determined by taking the average of micrometer measurements on 100 particles of each material. The average diameter of the alumina particles was found to be 0.0377 in. while that of the copper particles was found to be 0.0365 in. The alumina runs were made with 0.144 in. of inert oxide beads on each plate. In the copper study 0.072 in. of inert copper beads were used. The bulk densities for the inert bead materials were 1.5 g/cc for the glass, 5.4 for the copper and 0.72 for the alumina.

Figure 21 presents the results of the copper study. Comparison of the throughput rates found when using copper inert beads with those found when using glass beads reveals little difference in the throughput rates. In both cases, the throughput rates with copper were slightly smaller. In view of the fact that the "critical diameter" was larger in the case of the copper inert beads than for the glass beads the decrease in the throughput must be due to the high density of the copper beads. This would be expected because greater energy is necessary to impart motion to high density material than to low density material. Another factor involved in this decrease is the fact that the copper beads were not as spherical as the glass beads. Since the throughput rate decreased 15% on the average while the density of the inert material increased 3.5 times, it was concluded that the density of the inert material had little effect upon the throughput rate.

When the results of the alumina study (Figure 22) are compared with those obtained using glass beads (Figure 17), one finds that the throughput rates were greatly reduced (57%) when alumina was used for the inert beads. In this case the reduction in throughput rates is believed to have been caused by a reduction in the "critical diameter" caused by fracturing of the relatively soft alumina particles. Alumina fines were found in the inert-bead section of the plates after completion of the runs, thus confirming the cause.

From the above investigation it is concluded that the particle density of the inert material plays a minor role in determining the throughput rate. It reaffirmed the importance of the "critical diameter" and indicated the need for using spherical material for the inert beads.

(c) Diameter of the Inert Beads

The size of the inert beads is important in determining the largest particle that will pass downward through the plates in the column. In this work, 0.0357, 0.0592 and 0.188-in. diameter glass beads were used as inert material. The experimental data are presented in Figure 23 for the two larger beads. The data for the 0.0357-in. beads are presented in Figure 17. The data confirm the previous discussion (Section D-3), and will not be further discussed here.

5. Bed Depth Investigation

The effect of bed depth upon the throughput rate was investigated using No. 130 glass beads as feed, a superficial air velocity of 0.19 ft/sec and 0.144-in. depth of 0.0357-in. diameter glass spheres as inert material. Bed depths of 3, 5, 7, and 9 in. were

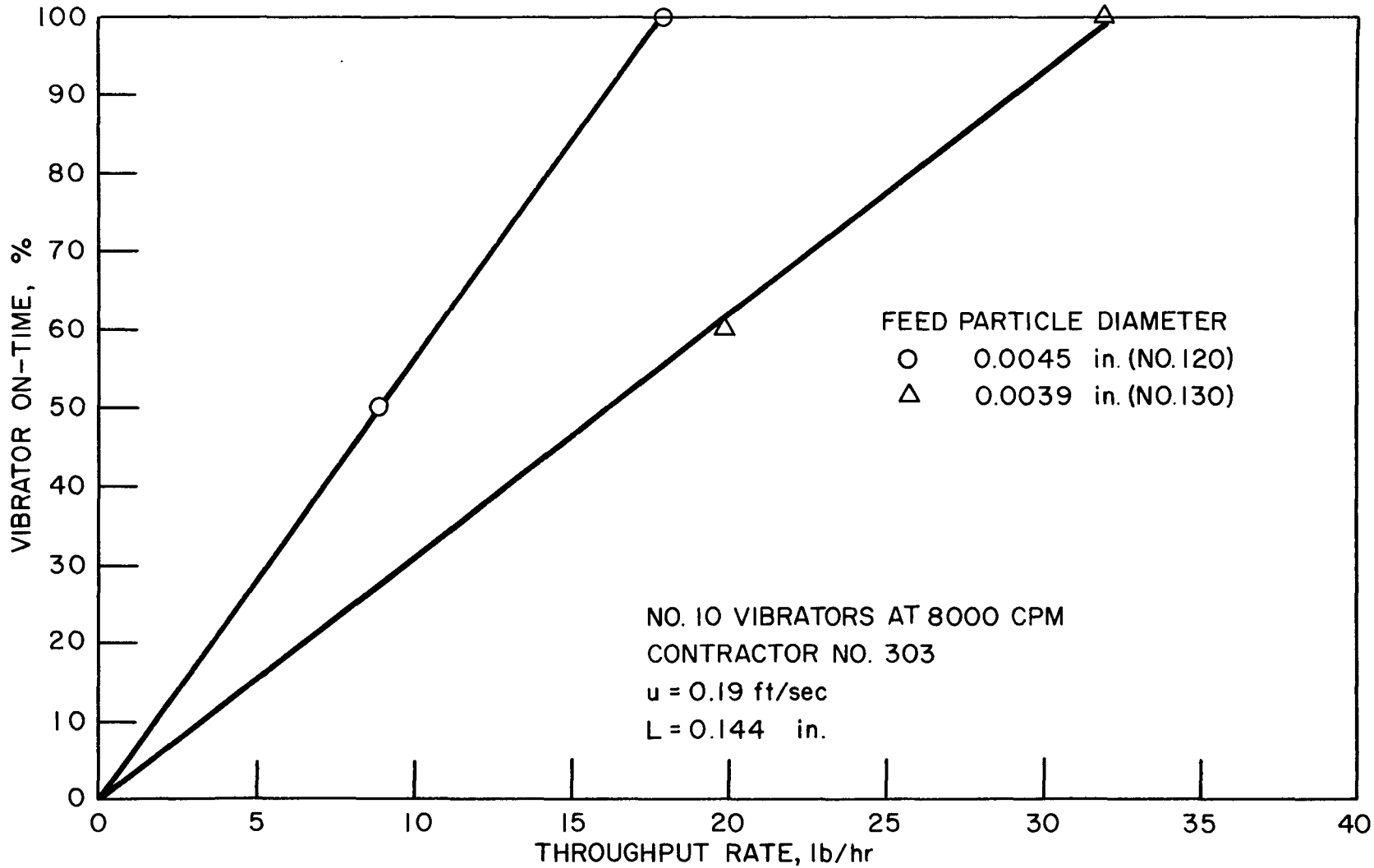

Figure 22. Vibrator On-time vs Throughput Rate with Alumina Inert Beads

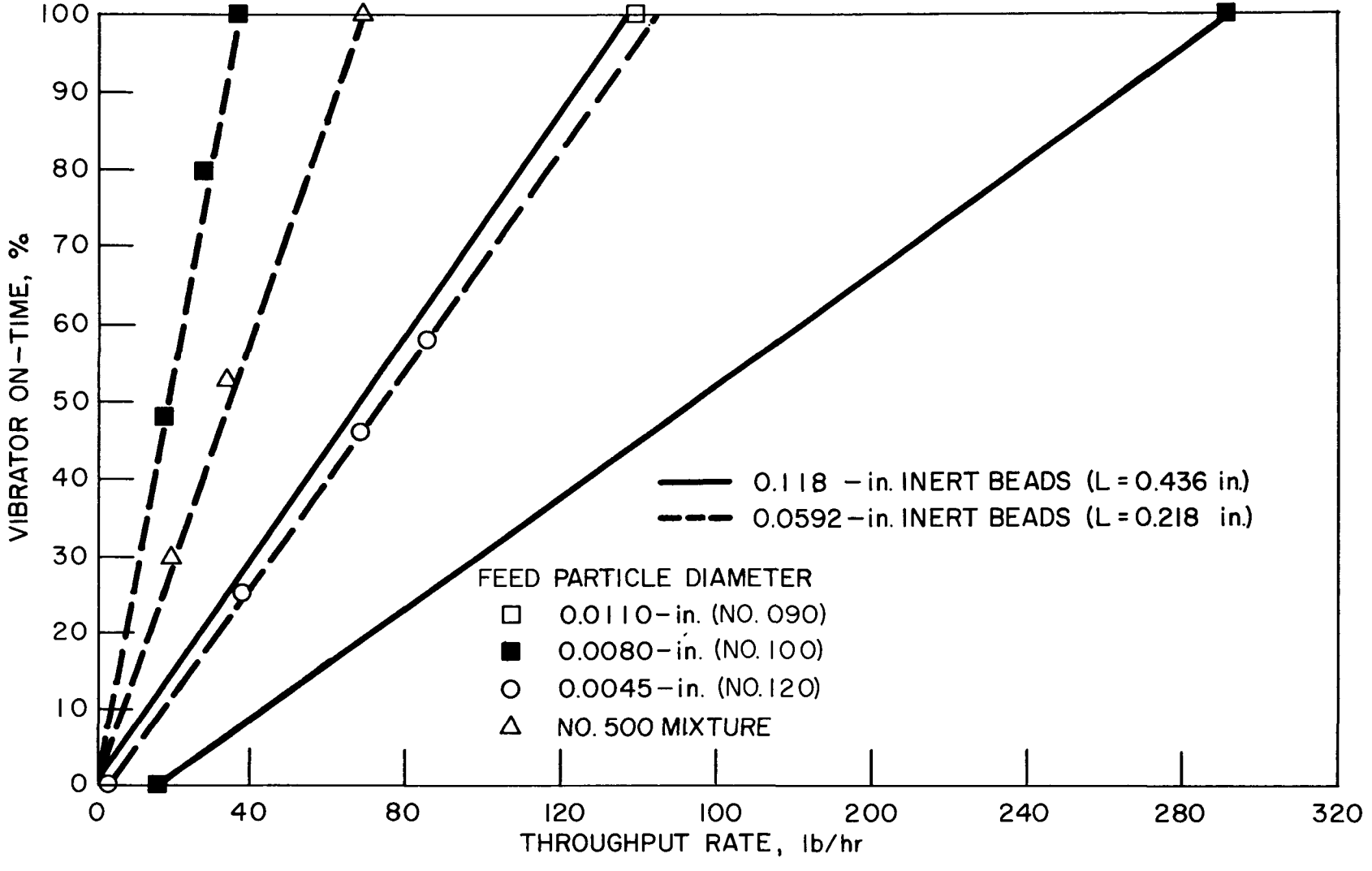

Figure 23. Vibrator On-time vs Throughput Rate with 0.0592 and 0.118-in. Diameter Inert Glass Beads

studied. These conditions are summarized in Table 7.

Table 7

Operational Study for Bed Depth Study

Cover and support plate	40 mesh screen, 13 mesh punched plate
Contactor	No. 303
Diameter of glass feed particles, D_p	0.0039 in. (No. 130)
*Bed depth, H	3, 5, 7, 9 in.
Superficial air velocity, u	0.19 ft/sec
Depth of inert beads, L	0.144 in.
Vibrators	BD-10 and BD-13
Vibrational frequency, S	8000 CPM
Run numbers	I908-920
Diameter of inert beads, D_I	0.0357 in. (glass)

* Variable for this study

The results are presented in Figure 24 as vibrator on-time versus the throughput rate and in Figure 25 as bed depth versus the maximum throughput rate. The range of bed depths studied correspond to depth over diameter ratios from 0.5 to 1.5. As seen in Figure 25, the throughput rate tends to decrease for bed depths less than 7 in. However, since this decrease is only 15 lb/hr in going from a 7 to a 2-in. bed, the throughput rate for engineering purposes can be considered independent of the fluidized bed depth. Above 7 in. the throughput rate was experimentally found to be independent of the fluidized-bed depth.

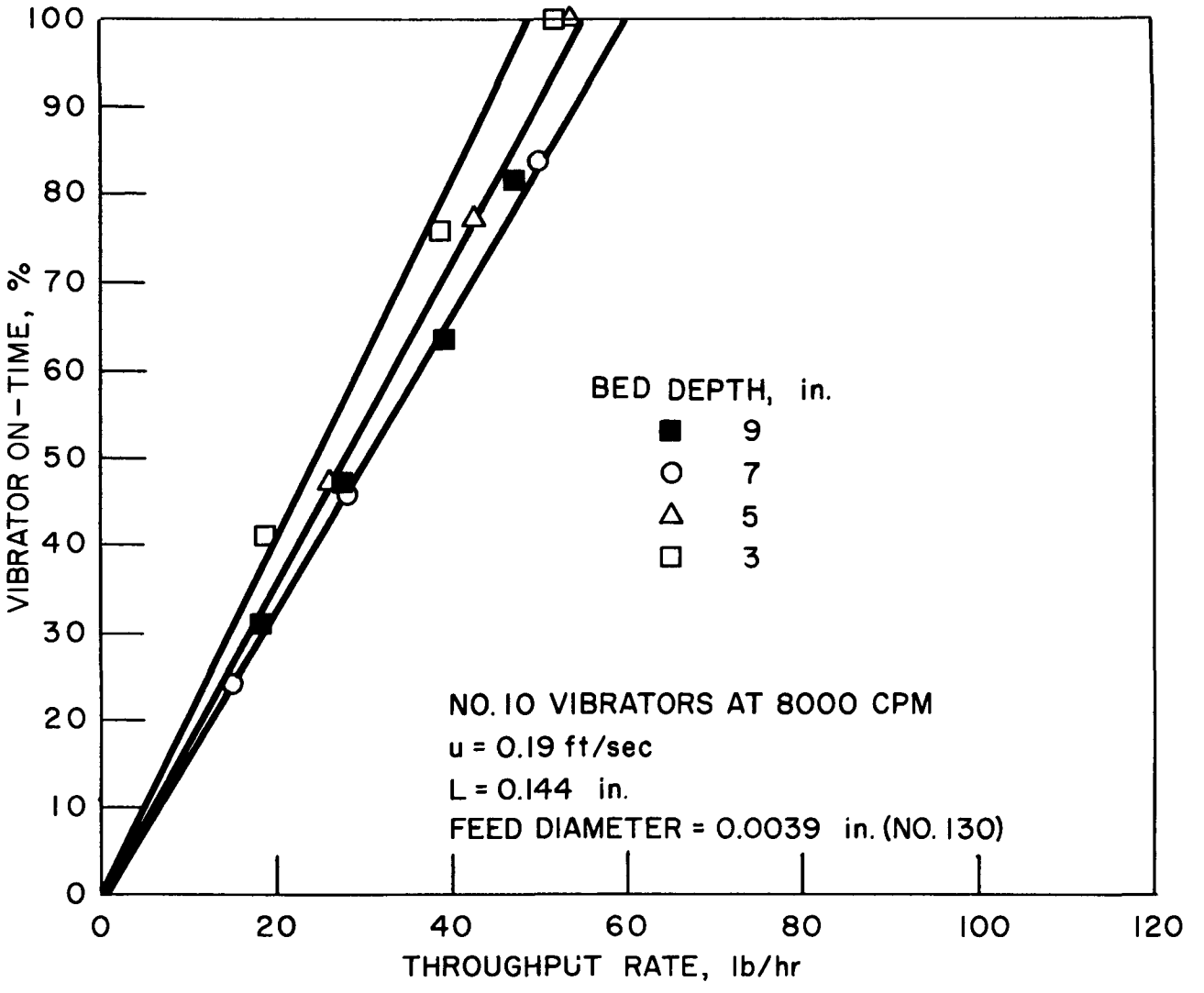

Figure 24. Vibrator On-time vs Throughput Rate with Bed Depth as the Parameter

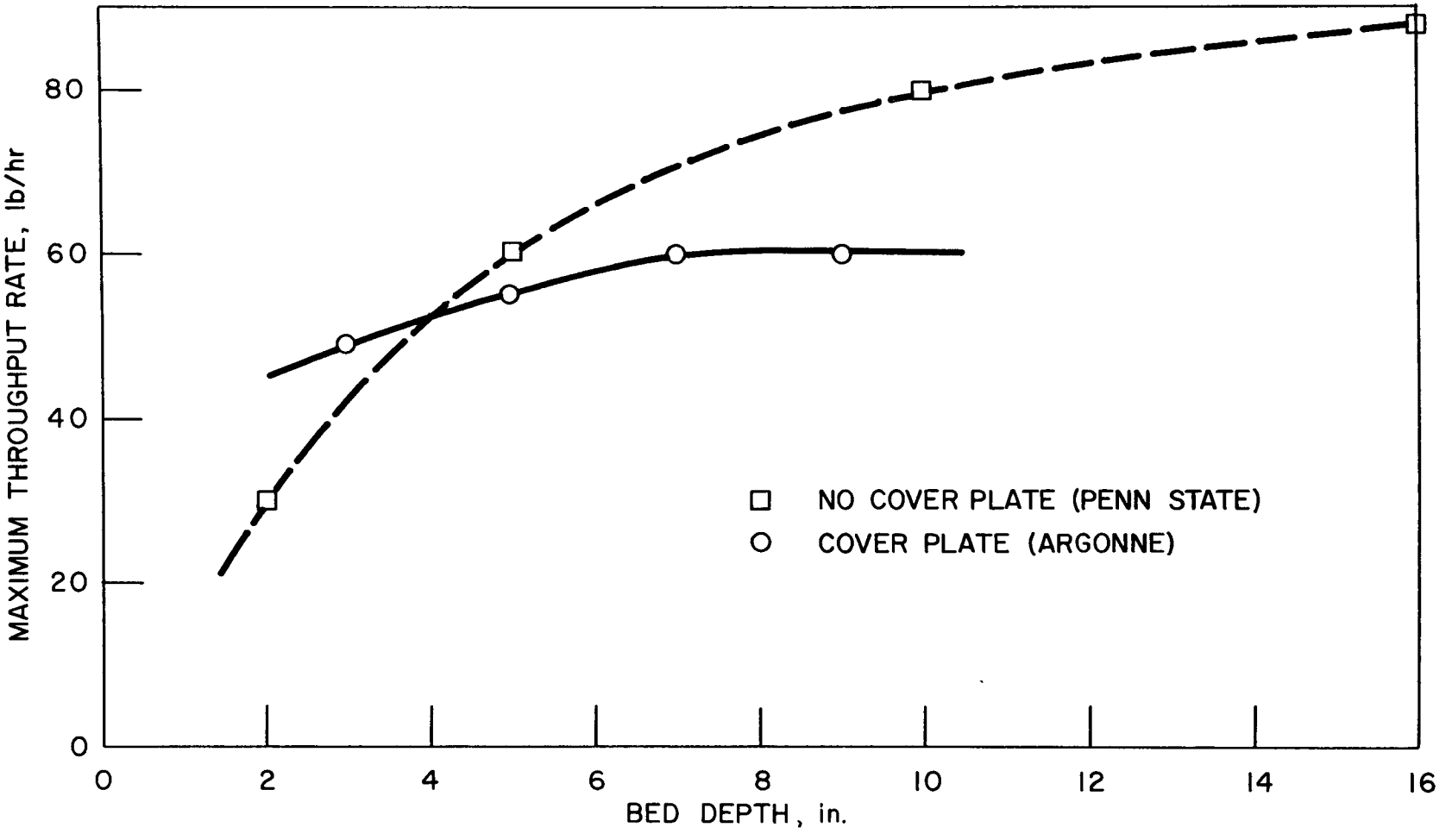

Figure 25. Maximum Throughput Rate vs Bed Depth

The depth of the fluidized bed was definitely a variable in the work conducted at The Pennsylvania State University[37]. Data for the Pennsylvania State University work are shown as the dashed line in Figure 25. The change in the status of fluidized-bed depth from a variable to a non-variable is accounted for by the use of a cover plate on each of the stages in the Argonne column. In the Pennsylvania State University column, the fact that bed depth was a variable can be explained as follows: With no cover plate present, the motion of the fluidized bed caused the inert beads to be thinned in spots thus baring the support plate and reducing the resistance offered by the inert beads to the downward transport of solids. As the beds became deeper the disturbance of the bead layer increased due to the increased bouncing action or motion of the fluidized bed. The latter was caused by the formation of rather large bubbles of fluidizing gas as the small bubbles coalesced while rising through the fluidized bed. In the Argonne column, the cover plate on each stage prevented, to a great extent, the eroding action of the fluidized bed. This led to much greater stability in the operation of the column.

6. Superficial Air Velocity Studies

The superficial air velocity investigation covered the range of velocities from zero to 0.5 ft/sec. The operational conditions are presented in Table 8. The results are presented in Figures 26, 27 and 28. The dashed line in each of the figures represents the minimum fluidization velocity. The minimum fluidization velocity was taken as that velocity at which the differential pressure across each plate suddenly decreased and leveled off to a constant value. At this

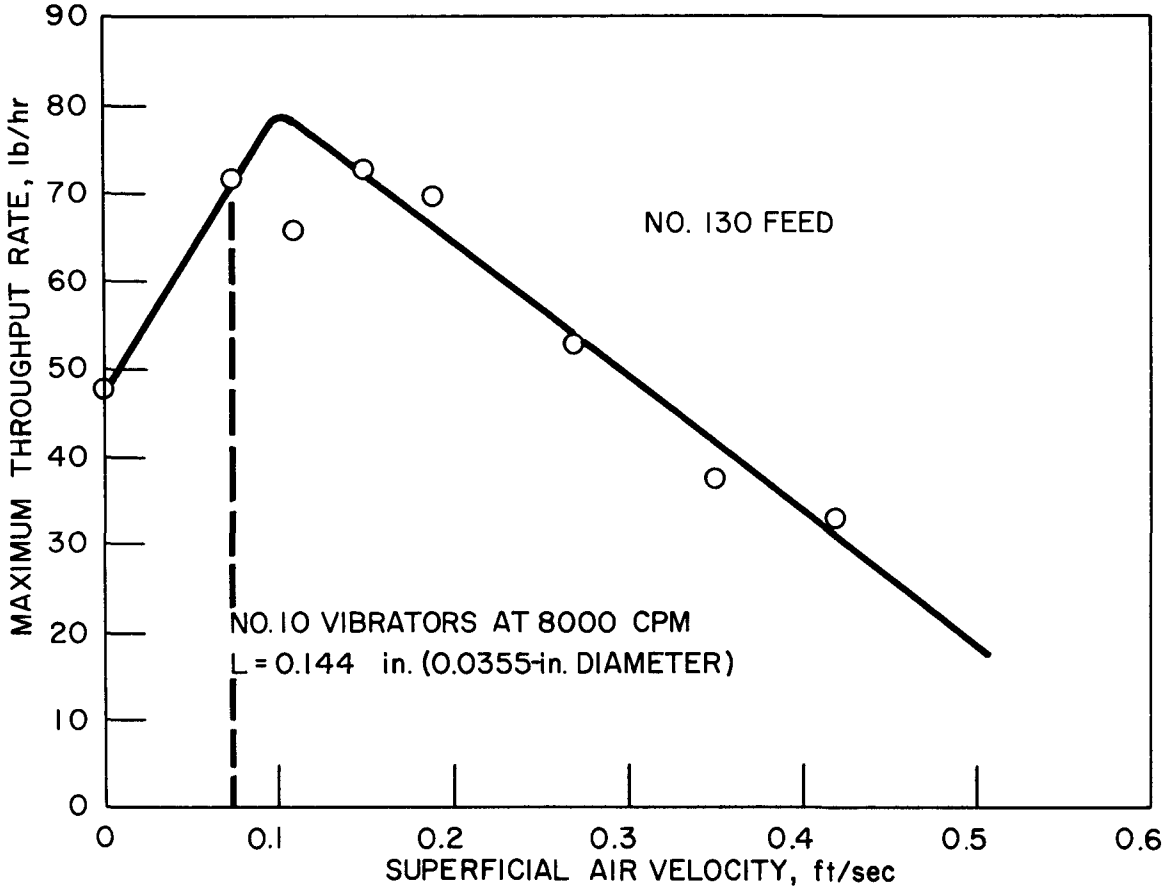

Figure 26. Maximum Throughput Rate vs Superficial Air Velocity for No. 130 Feed Material

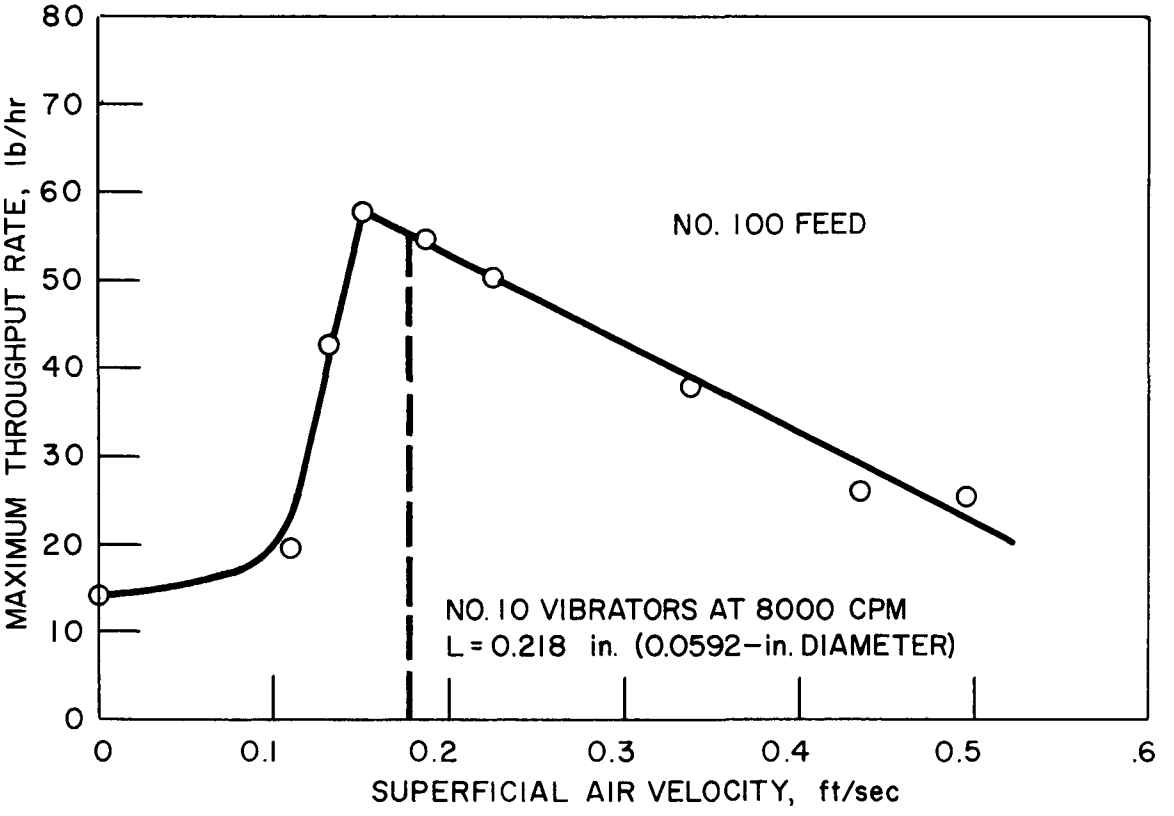

Figure 27. Maximum Throughput Rate vs Superficial Air Velocity for No. 100 Feed Material

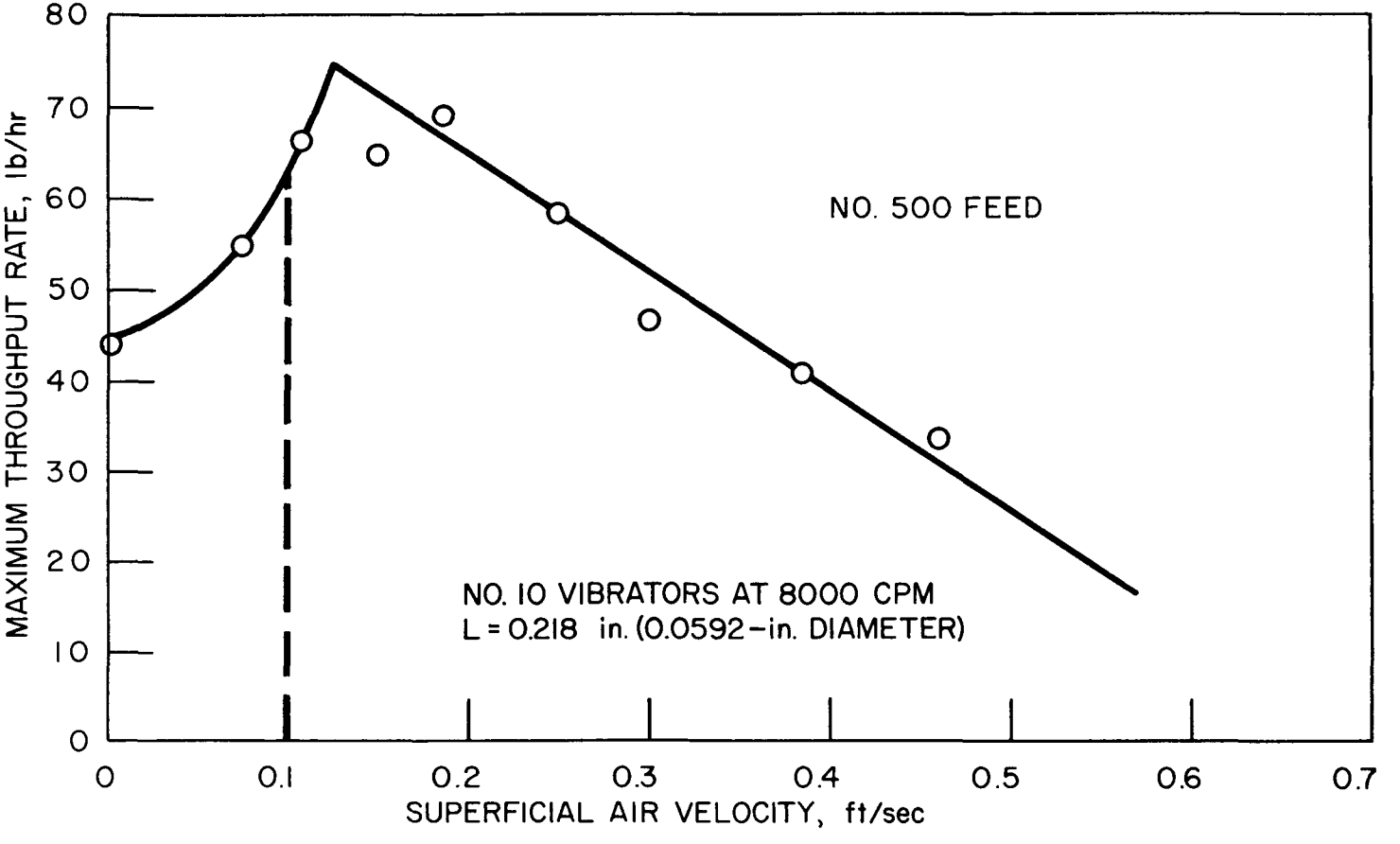

Figure 28. Maximum Throughput Rate vs Superficial Air Velocity for No. 500 Feed Material

velocity, the first gas bubbles appeared on the surface of the "fluidized" bed.

Table 8

Operational Conditons for Superficial Air Velocity Study

Cover and support plate	40 mesh screen, 13 mesh punched plate
Contactor	No. 303
Diameter of glass feed particles, D_p	0.0069 to 0.0080 in. (No. 100, 130, 500)
Bed depth, H	7 in.
Superficial air velocity, u	0.0 to 0.5 ft/sec
Depth of inert beads, L	0.144 in.
Vibrator	BD-10
Vibrational frequency, S	8000 CPM
Run numbers	I801-846, I500-502, I549
Diameter of inert beads, D_I	0.0357 and 0.0592 in. (glass)

In Figures 26, 27, and 28 it can be seen that the maximum throughput rate decreased linearly as the superficial air velocity was increased from a value approximating that of the minimum fluidization velocity. As the superficial air velocity increased from zero to that required for minimum fluidization to occur, the maximum throughput rate increased but not linearly.

Let us now examine the reasons for this behavior. The kinetic energy of the fluidizing gas is $\frac{u^2}{2g_c}$ (expressed as feet of fluid flowing). When expressed as a pressure, the kinetic energy is referred to as velocity pressure (P_v) and is defined as follows:

$$P_v = u^2 \rho_g / 2g_c \qquad (7)$$

This so called velocity pressure is exerted upon each of the feed particles. At the same time, each of the feed particles exerts a force opposite to that of the flowing air due to the action of gravity upon its mass. If we assume spherical feed particles the velocity pressure of the fluidizing gas will counteract the particle pressure, P_p, based upon the cross-section area of the particle. The downward particle pressure based upon its cross-sectional area is:

$$P_p = \frac{(\rho_p)(\frac{1}{6})(\pi D_p'^3)(g)}{(\frac{\pi D_p'^2}{4})(g_c)} = \frac{2}{3} \rho_p D_p' (g/g_c) \qquad (8)$$

With a superficial air velocity of zero, throughput is achieved because part of the vibrational energy is utilized in loosening the packed bed of feed material. As the velocity pressure is slowly increased by increasing the superficial air velocity, larger and larger fractions of the particle pressure are counterbalanced thus allowing more and more freedom of movement in the "prefluidized" bed. This increased freedom of movement reduces the clogging effect in the inert bed layer and allows higher throughput rates. This continues until a peak in the throughput curve is reached. At the peak the superficial air velocity is such that there is maximum freedom of particle movement with the velocity pressure not greater than the particle pressure. In actuality the velocity pressure should be approaching the particle pressure. Further increases in the velocity pressure cause the bed to undergo vertical movement in which the feed

particles are shoved away from the plate. This results in decreased throughput because the particles are now suspended and carried upward in the fluidizing gas stream.

For the reasons discussed above, the peak throughput rate will occur at a superficial air velocity determined by equating velocity pressure to particle pressure as follows:

$$\frac{P_v}{P_p} = A' = 0.335 \times 10^{-3} \qquad (9)$$

In this equation A' is a constant which was evaluated from the experimental values of P_v and P_p. The superficial air velocities used to calculate A' are designated as u_m and are based upon the total cross-sectional area of the column (0.196 ft^2). When A' is calculated from an air velocity based upon the free area existing at any level within the inert bead layer (0.042 ft^2) assuming no feed particles present, the pressure ratio has a value of 0.725×10^{-2}. If it is assumed that spherical feed particles (with a diameter equal to the critical diameter) fill the interstitial volume between the inert beads, the cross-sectional area is further reduced (to 0.034 ft^2) and the pressure ratio increased to 0.0111. The calculation of A' is presented in Appendix I.

Using the relationship developed in Equation 9 it is possible to determine the superficial air velocity, u_m, at which maximum throughput will occur for any given spherical feed particle. To account for non-spherical particles a shape factor (ϕ_s) is included. The use and evaluation of the shape factor is discussed in Part V, Section C. In its final form, Equation 9 becomes:

$$\frac{P_v}{P_p} = \frac{u_m^2 \rho_g \phi_s}{1.34 g \rho_p D_p'} \tag{10}$$

When this equation is solved for u_m we get:

$$u_m = (1.20 \times 10^{-3})(\rho_p \rho_g^{-1} D_p \phi_s^{-1})^{1/2} \tag{11}$$

In this equation the average feed particle, D_p, is in inches.

The fact that throughput decreases linearly for superficial vapor velocities greater than u_m enables an equation to be empirically derived which relates the throughput rate at u_m to the throughput rate at any velocity greater than u_m. The average slope of the lines in Figures 26, 27, and 28 was found to be -127 lb-sec/hr-ft. Therefore by definition of the slope:

$$(W_L^{u_m} - W_L^u)/(u_m - u) = \text{slope} = -127 \tag{12}$$

Solving for the throughput rate, W_L^u, gives:

$$W_L^u = W_L^{u_m} - 127\ (u - u_m) \tag{13}$$

Equation 11 can then be substituted into Equation 13. With Equation 13, the throughput rate at any L and u can be converted to the throughput rate obtainable at u_m and the same L. Calculation of the throughput rate at u_m is of value because the design correlation (Part V) is based upon the air velocity, u_m.

It is interesting to compare these results with those obtained on the column constructed and operated at The Pennsylvania State University[37]. In the Pennsylvania State University column

increases in the superficial air velocity were accompanied by increases in the throughput rates. The difference in operation between the two columns is due to the incorporation of a cover plate in the Argonne equipment. The effect of this plate was discussed under Section D-5.

7. Uncontrolled Throughput

Data on uncontrolled throughput rates were obtained throughout the experimental investigation of the column variables already discussed. Uncontrolled throughput is that downward transport of solids which takes place without the vibrators in operation. On the basis of glass beads, uncontrolled throughput rates in excess of 5 lb/hr were considered to be undesirable. On the plots of vibrator on-time versus throughput rate such as Figure 18, the uncontrolled throughput rates were found at the x-axis intercepts, i.e. the throughput rates at zero vibrator on-time. The influence of air velocity upon the uncontrolled throughput rate is shown in Figure 29. Data for this figure were obtained with plates containing 0.072 and 0.144 in. of 0.0357-in. diameter inert beads. Glass beads were used as the feed. As seen in this figure, the uncontrolled throughput rate increases very rapidly as the vapor velocity is increased when the inert bead layer is only 0.072-in. thick. However, in the runs using 0.144 in. of inert material, the uncontrolled throughput rate was found to be essentially independent of the air velocity. The fact that the uncontrolled throughput rate increased as the air velocity increased in the former case is attributed to the fact that plates with only approximately 1/16th inch of inert material tended to be non-uniform in resistance to the downward flow of particles. From these findings, it is recommended that inert bead depths greater than 0.109 in. be used in

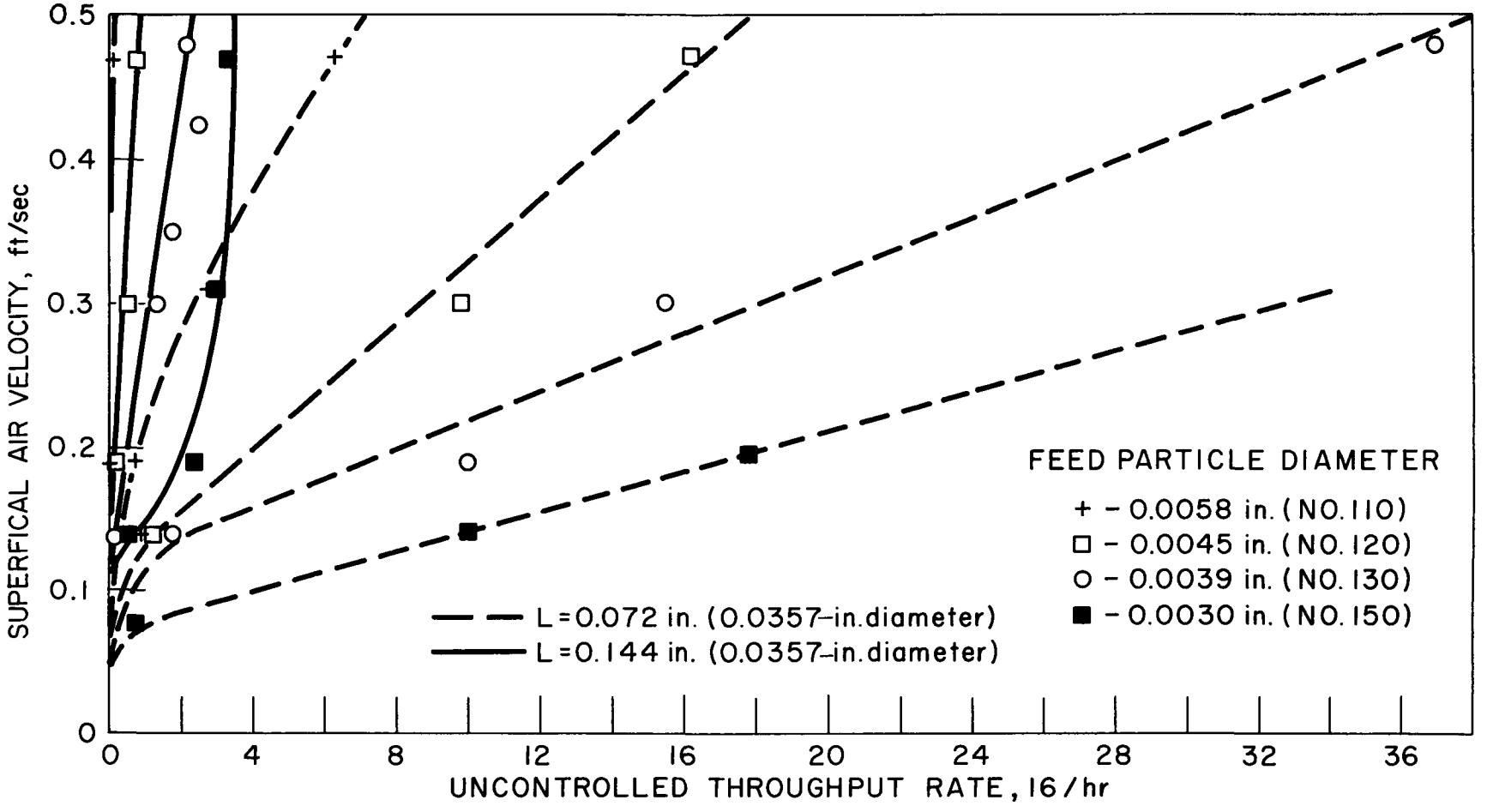

Figure 29. Superficial Air Velocity vs Uncontrolled Throughput

any column construction in order to eliminate the velocity dependence described above.

The uncontrolled throughput rate was also found to be dependent upon the difference between the "critical diameter" and the average feed diameter. This dependence is shown in Figure 30 as a plot of diameter differences versus the depth of inert beads on each plate. If the difference in diameters fell above the line in this figure for the given depth of inert beads, then the uncontrolled throughput rate was found to be in excess of 5 lb/hr. Points beneath the line resulted in uncontrolled throughput rates of less than 5 lb/hr. Figure 30 is assumed to be valid for any vapor velocity as long as L is greater than 0.109 inches.

Equation 11 is used to calculate the superficial air velocity at which the maximum throughput rate occurs.

$$u_m = (1.23 \times 10^{-3})(\rho_p \rho_g^{-1} D_p \phi_s^{-1})^{1/2} \qquad (11)$$

Equation 13 relates the effect of air velocity to the throughput rate.

$$W_L^u = W_L^{u_m} - 127\ (u - u_m) \qquad (13)$$

The above equations were derived on the basis of the following conditions:

Feed ..... glass beads

Column ..... 6-inch diameter

Vibrators ..... BD-10 at 8000 CPM operating 100% of the time

In order to give the correlation more general use, an equation can be derived to relate the throughput rate of any material in any size column with any vibrator on-time to that of glass beads in a 6-in. column with the vibrators operating 100% of the time. The derivation of this equation follows: Throughput rates expressed as lb/hr are not constant as the feed material is varied because of feed density variations. However, throughput rates expressed as $ft^3/hr\text{-}ft^2$ column cross-sectional area are constant. For glass beads in a 6-in. diameter column:

$$\frac{W_L^u}{A_6 \rho_{gl}^b} = Y\ ft^3/hr\text{-}ft^2 \qquad (15)$$

In which A_6 is the cross sectional area of the 6-in. column and ρ_{gl}^b is the bulk density of the glass beads.

For any other material in any size column:

$$\frac{w_L^u}{A\rho} = X \text{ ft}^3/\text{hr-ft}^2 \tag{16}$$

Equating X and Y:

$$\frac{W_L^u}{A_6 \rho_{gl}^b} = \frac{w_L^u}{A\rho} \tag{17}$$

Solving for W_L^u and substituting for A_6 and ρ_{gl}^b:

$$W_L^u = \left(\frac{A_6 \rho_{gl}^b}{A\rho}\right) w_L^u = \frac{(0.196 \text{ ft}^2)(1.5 \text{ g/cc})}{A\rho} w_L^u = \left(\frac{0.292}{A\rho}\right) w_L^u \tag{18}$$

To correct the desired operating throughput rate at a given vibrator on-time to that occuring with the vibrator operating 100% of the time, Equation 19 is modified by the addition of the desired vibrator on-time, t, as shown in Equation 19. This is valid since the vibrator on-time was found to be a linear function of the throughput rate.

$$W_L^u = \frac{29.2}{A\rho t} w_L^u \tag{19}$$

In order to calculate the diameter of the inert beads directly it is necessary to substitute Equation 3 into Equation 14. Equation 20 results from this substitution.

$$D_I = 6.46 D_p \phi_s + 2.18 \times 10^{-4} W^{u_m}_{.218} - 2.98 \times 10^{-3} \tag{20}$$

B. Limitations of the Correlation

The limiting values of the variables listed were determined by the extent of the experimental investigation. In many cases it is

felt that the limiting values could be extended.

Feed material ..... any (no restrictions)

Fluidized bed depth ..... >3 in.

Throughput rates ..... up to 15 $ft^3/hr\text{-}ft^2$

Fluidizing gas velocity ... $u_m = u = 5u_m$

Amount of inert material .. 0.109 in. $\leqq L \leqq$ 0.436 in.

Vibrators ..... BD-10 at 8000 CPM

Shape of inert material ... spherical only

C. Discussion of the Correlation

The correlation is felt to be valid for many types of feed materials. (Activated alumina and silica gel were used to test the correlation). The shape of the feed particles has been accounted for by the inclusion of a shape factor. The factor used is that defined by Leva[14]. Typical values range from 1 for spheres and 1.16 for round sand to 1.73 for cracking catalyst. Since there is no easy way to calculate the shape factor for jagged particles, Leva suggests comparison of the feed material of unknown shape factor with that of photos[14,15] for materials of known shape factor. From a comparison of the photos an approximate shape factor can be determined for the unknown material.

To substantiate the general application of the correlation, runs were made using alumina and silica gel as the feed materials. The oxide had a bulk density of 55 lb/ft^3 and a shape factor (as determined by Leva's method) of 1.62; the gel a bulk density of 45 lb/ft^3 and a shape factor of 1.40. Photos of the three feed materials are shown in

Figure 32. The experimental throughput rates were 33.4 lb/hr for the alumina and 5.8 lb/hr for the gel. The correlation predicted throughput rates of 35 lb/hr for the alumina and 5.3 lb/hr for the gel. The results of these runs are included in Figure 31.

In determining the average particle diameter of the feed the weight mean average was used. It should be emphasized that the largest particle in any feed, when multiplied by its shape factor, must have a diameter in the order of the "critical diameter". If a substantial number of the feed particles are larger than the "critical diameter" the plates will clog and no throughput will be obtained. On the other hand, an average particle diameter considerably smaller than the "critical diameter" will cause uncontrolled throughput. One set of runs was made using a specially prepared glass bead mixture (No. 500) which contained a wide particle size distribution (from 50 to 400 mesh). The calculated throughput rate of 74.6 lb/hr was 6.6 lbs more than the actual rate of 68 lb/hr. (See Figure 31).

The effect of vibrational frequency was not included in the correlation in order to incorporate a safety factor into the calculations. As discussed in Part IV, Section D, increases in vibrational frequency cause increased throughput rates of as much as 20%. If in actuality the throughput rates are less than desired, they can be increased by increasing the vibrational frequency above the 8000 CPM used for the correlation.

The inert glass beads were obtained from the A. S. Lapine Co. of Chicago, Illinois, in closely graded sizes of 1/2, 1, 1-1/2, 2, 2-1/2, and 3 mm diameter. Because the sizes available differ by 1/2 mm, it is advisable to use inert beads next largest to that calcu-

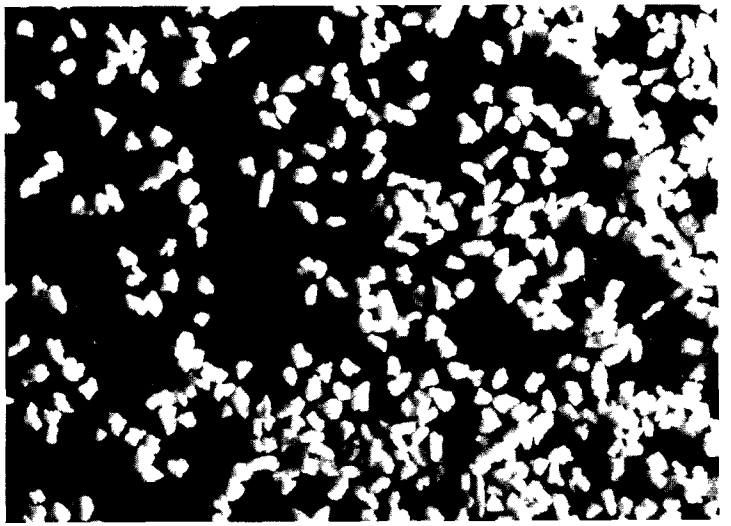

ALUMINA

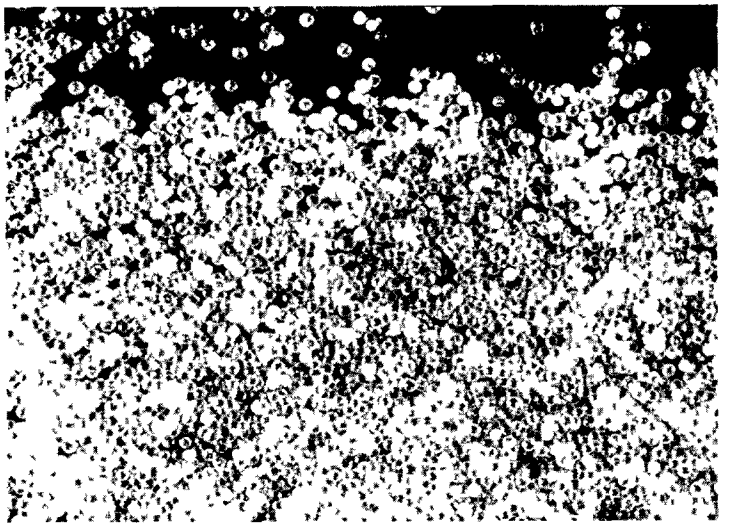

GLASS BEADS

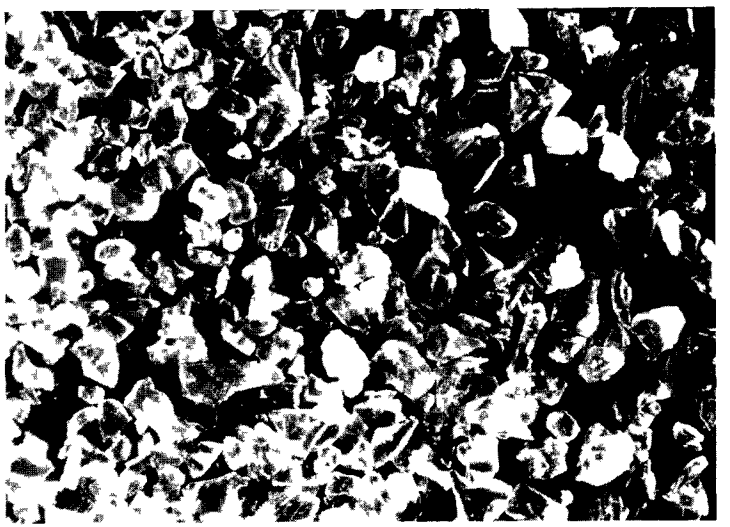

SILICA GEL

Figure 32. Photographs of the Feed Materials

lated by Equation 20. This will result in a greater than desired throughput rate, which will automatically be corrected by a reduction of the vibrator on-time. This procedure incorporates another safety factor into the calculations.

A comparison of the experimental and the calculated values of the throughput rates is presented in Appendix I. An average deviation of 4.7 lb/hr between the calculated and experimental throughput rates was found. Based upon the average throughput rate of 71.7 lb/hr this gave an average deviation of 6.5%.

D. Procedure for Using the Correlation

The following procedure is based upon the assumption that the designer wants to know what size inert beads is necessary to achieve a desired throughput rate for a particular feed while the column is operating under known conditions (vapor velocity, vapor density, etc). If the requirement is to know the throughput rate for a particular material using an already existent column, the procedure would be identical but carried-out in reverse order.

Step 1: From Equation 18, the throughput rate based upon glass beads is determined. This throughput rate is for the desired superficial vapor velocity, u, and depth of inert beads, L. It is recommended that the value of L be arbitrarily chosen as 0.218 in. as this insures stable plate operation. We have therefore calculated $W^{u}_{.218}$.

Step 2: The superficial vapor velocity at which maximum throughput occurs is then calculated from Equation 11. This equation, 11 , utilizes the physical properties of the fluidizing gas and the feed material.

Step 3: Equation 13 is now used to correct the throughput rate at superficial vapor velocity, u, to that occuring at u_m. Since the depth of inert beads was chosen to be 0.218 in. this calculation gives us $W^{u_m}_{.218}$. If we had not chosen L equal to 0.218 in. Equation 6 would have to be used prior to the next step.

Step 4: Finally Equation 20 is used to calculate the diameter of the inert beads, D_I. The actual diameter of the inert beads used is the nearest 1/2 mm larger bead than the calculated value, D_I.

Step 5: In order to determine if these conditions will result in too much uncontrolled throughput, use is made of Figure 30. If the diameter difference, $(D_I/6.46) - D_p\phi_s$, falls above the line in this figure for L equal to 0.218 in. then the uncontrolled throughput rate will be greater than 5 lb/hr (based on glass beads density). If this is the case, L should be increased and the above calculation procedure repeated using the new value of L. If the point falls below the line, uncontrolled throughput will be less than 5 lb/hr and no further calculations are then necessary.

E. Sample Calculation

It is desired to dehumidify air using activated alumina. The desired operating conditions are as follows:

Feed: activated alumina	ρ_g = 0.0742 lb/ft^3 (air)
ρ = 0.875 g/cc	Column: 6-in. diameter
ρ_p = 100 lb/ft^3	u = 0.15 ft/sec
D_p = 0.0045-in. diameter	w^u_L = 40 lb/hr
ϕ_s = 1.62	t $\leq$ 80%

Find: D_I and L to give the required throughput rate.

Step 1: Assume the inert bead depth (L) equal to 0.218 in.

Step 2: Calculate $W^u_{.218}$ from Equation 18:

$$W^u_{.218} = \frac{29.2(40)}{0.196(0.875)(80)} = 85 \text{ lb/hr}$$

Step 3: Calculate u_m from Equation 11:

$$u_m = (1.23 \times 10^{-3})(\rho_p \rho_g^{-1} D_p \phi_s^{-1})^{1/2} = \sqrt{\frac{1.2 \times 10^{-3}(100)(0.0045)}{0.0742)(1.62)}}$$

$$u_m = 0.072 \text{ ft/sec}$$

Step 4: Calculate $W^{u_m}_{.218}$ from Equation 13:

$$W^{u_m}_{.218} = W^u_{.218} + 127(u - u_m)$$

$$= 85 + 127(0.15 - 0.072)$$

$$= 95.8 \text{ lb/hr}$$

Step 5: Calculate D_I from Equation 20:

$$D_I = 6.46 D_p \phi_s + 2.18 \times 10^{-4} W^{u_m}_{.218} - 2.98 \times 10^{-3}$$

$$= 6.46(0.0045)(1.62) + 2.18 \times 10^{-4}(95.8) - 2.98 \times 10^{-3}$$

$$= 0.0651 \text{ in. or } 1.65 \text{ mm}$$

Since the inert beads are available in 1/2 mm sizes, choose 2 mm beads for the inert material.

Step 6: Check Figure 30 for uncontrolled throughput:

$$D_I/6.46 - D_p \phi_s = 2/(25.4)(6.46) - 0.0045(1.62) = 0.0048 \text{ in.}$$

For L equal to 0.218 in. the point falls above the line.

Therefore the uncontrolled throughput rate will be >5 lb/hr.

Step 7: Revise L by consulting Figure 30 and recalculate back to w^u_L to determine if t (the vibrator on-time) will still be equal to or less than 80% for a throughput rate of 40 lb/hr. Let L equal 0.327 in. (Point now under the line in Figure 30)

Step 8: Calculate $W^{um}_{.218}$ from Equation 20 using D_I equal to 2 mm:

$$0.0788 = 0.0472 + 2.18 \times 10^{-4} W^{um}_{.218} - 2.98 \times 10^{-3}$$

$$W^{um}_{.218} = 159 \text{ lb/hr}$$

Step 9: Calculate $W^{um}_{.327}$ from Equation 6:

$$W^{um}_{.327} = W^{um}_{.218} - 100 + \exp(4.04 - 0.368 \ln L)$$

$$= 159 - 100 + \exp(4.04 - 0.368 \ln 0.327)$$

$$= 159 - 100 + 87 = 146 \text{ lb/hr}$$

Step 10: Calculate $W^u_{.327}$ for u equal to 0.15 ft/sec (use Equation 13):

$$W^u_{.327} = 146 - 127(0.15 - 0.072)$$

$$= 136 \text{ lb/hr}$$

Step 11: Calculate $w^u_{.327}/t$ from Equation 18:

$$\frac{w^u_{.327}}{t} = \frac{W^u_{.327}(A\rho)}{29.2} = \frac{136(0.196)(0.875)}{29.2} = 0.796$$

Using the desired throughput rate ($w^u_{.327}$) of 40 lb/hr, the above equation is solved for t, the vibrator on-time.

$$t = 50.2\% \text{ which is } < 80\%$$

Step 12: The final design conditions will then be:

$L = 0.327$ in. $\quad t = 50\%$

$D_I = 2$ mm $\quad w^u_L = 40$ lb/hr

VI. PART I - CONCLUSIONS

The following conclusions were drawn from the operation of a newly designed three-stage, fluidized-bed reactor.

1. The incorporation of a cover plate into each stage results in improved column stability.
2. The use of internal vibration allows individual control of the throughput of each plate.
3. Bed depth can be controlled to within one-half inch of any desired depth by controlling vibrator operation in accordance with the differential pressure across each stage and its bed.
4. A design correlation has been developed which permits the calculation of the column variables necessary to achieve the desired throughput of any feed material.

VII. PROCESS APPLICATIONS

Generally speaking, the equipment discussed in this thesis would have application in any gas-solid reaction in which counter-current flow is desirable. This equipment would also be useful where it is advantageous to maintain temperature gradients in order to effect a clean-up of residual reactant.

Specific application discussed in the literature and summarized by Zenz and Othmer[39] include the reduction of iron ore with hydrogen to produce sponge iron and with carbon monoxide to produce Fe_3C; the continuous drying of cement rock, coal and table salt; the reduction of uranium trioxide to uranium dioxide with hydrogen; the roasting of pyritic ores, gold ores and limestone; the retorting of oil shales; the fluorination of hydrocarbons in cobalt trifluoride beds; the calcination of low grade manganese ores; the chlorination of titanium ores; and the recovery of zinc from sulfide concentrates by chlorination.

PART 2.

MASS-TRANSFER STUDY

VIII. PART 2. -- MASS TRANSFER STUDY

A. Introduction

The purpose of this phase of the work was to obtain experimental mass-transfer data using the newly designed multistage fluidization column, and if possible to make a comparison of the operation of this column with other fluidized-bed units. For this study the silica-gel water-vapor adsorption system was chosen, because it lends itself readily to the fluidization technique and presents no difficult analytical problems.

Several mass-transfer studies have been reported in the literature (2,3,7,8,12,32,33). Of these the works of Cox (3) and Etherington (7) are of most interest in the present study. Cox calculated mass-transfer coefficients for the silica-gel water system from data obtained on a pilot-plant-size multistage fluidization column equipped with downcomers. His purpose was to show the possibility of using fluidization in the large scale drying of air. He found that the mass-transfer coefficient decreased as the bed depth increased. Etherington calculated Murphree vapor efficiencies for a multistage unit in which C_1, C_2 and C_3 hydrocarbons were adsorbed on activated charcoal. He reported efficiencies of nearly 100% at high vapor velocities and nearly 70% for velocities in the minimum fluidization range. Gas distribution problems were encountered in this study.

B. Scope

The equilibrium relationship between silica gel and water vapor was determined for temperatures from 20 to 40 ^{o}C and pressures from atmospheric to 20 psia. These data were then used

to evaluate the Murphree vapor efficiency for the adsorption of water vapor from air by silica gel in the six-inch multistage fluidization column. From the efficiency a modified mass-transfer coefficient was calculated. Runs were made at bed depths from 3/4 in. to 8 in. and superficial air velocities from 0.20 to 0.98 ft/sec.

C. Equilibrium Experiments

1. Equipment

The equilibrium experiments were carried out in a 2-in. I. D. glass column (see Figures 33 and 34). The fluidized silica-gel bed was supported by a wire screen which had openings smaller than the gel particles. There were no inert beads present. However, the fluidization was good because of the relatively high air velocity (0.45 ft/sec) and small column diameter. Gel samples were removed from the column through a Tygon tube. The bed temperature was determined from a thermometer placed in the bed. To obtain equilibrium data at elevated temperatures a resistance heating tape was used. This tape was wound around the outside of the glass column and its power input was controlled by a Variac. The humidifiers described in Part III (See Figure 5) were used to obtain the desired absolute humidity and the General Electric dew point recorder continuously monitored the water content of the fluidizing air.

2. Procedure

Two to three inches of activated silica gel were placed in the 2-in. column. The fluidizing air was then turned on and adjusted to the desired absolute humidity by regulating the

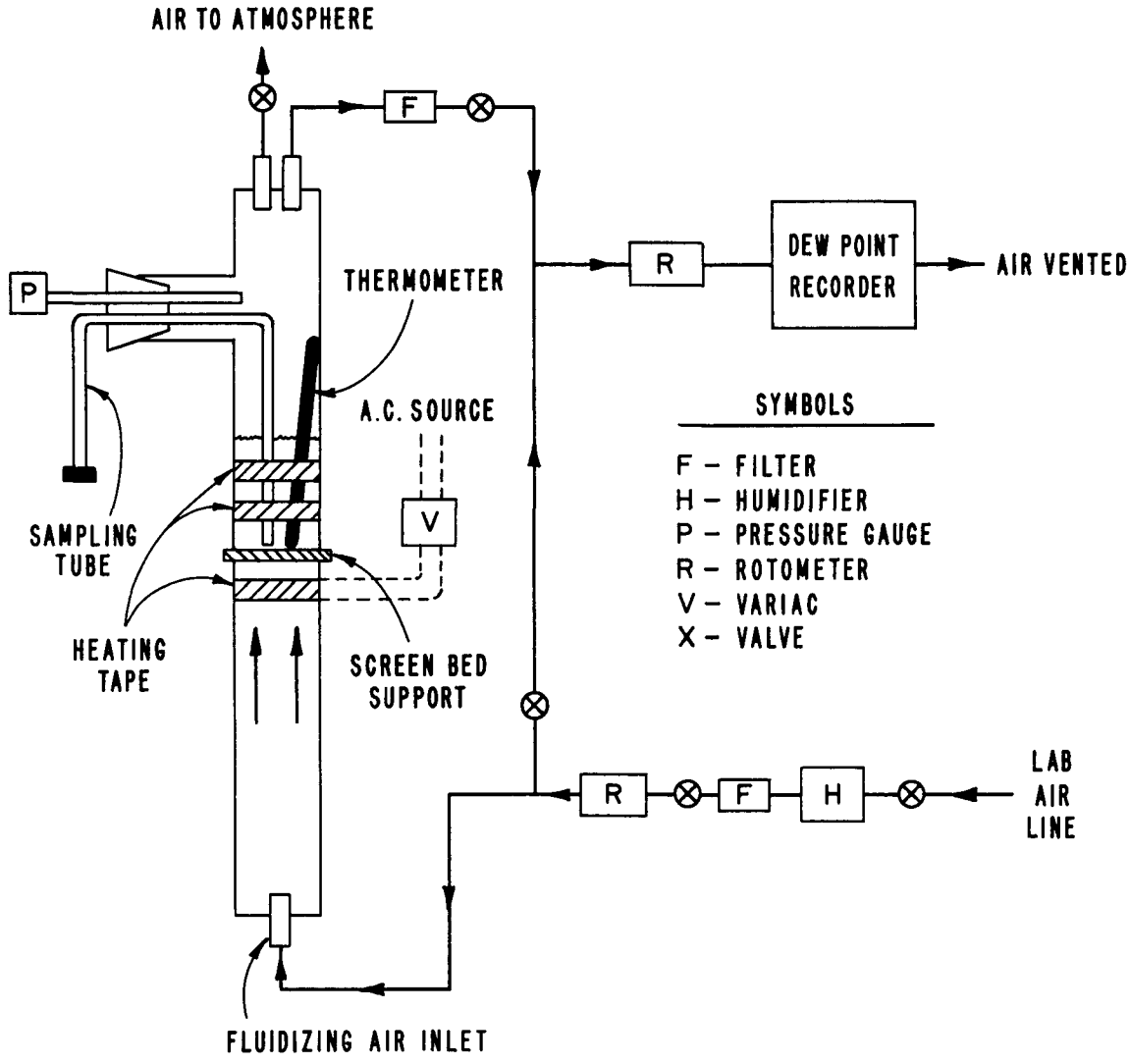

Figure 33. Schematic Diagram of the 2-in. Diameter Glass Column Used to Obtain the Equilibrium Data

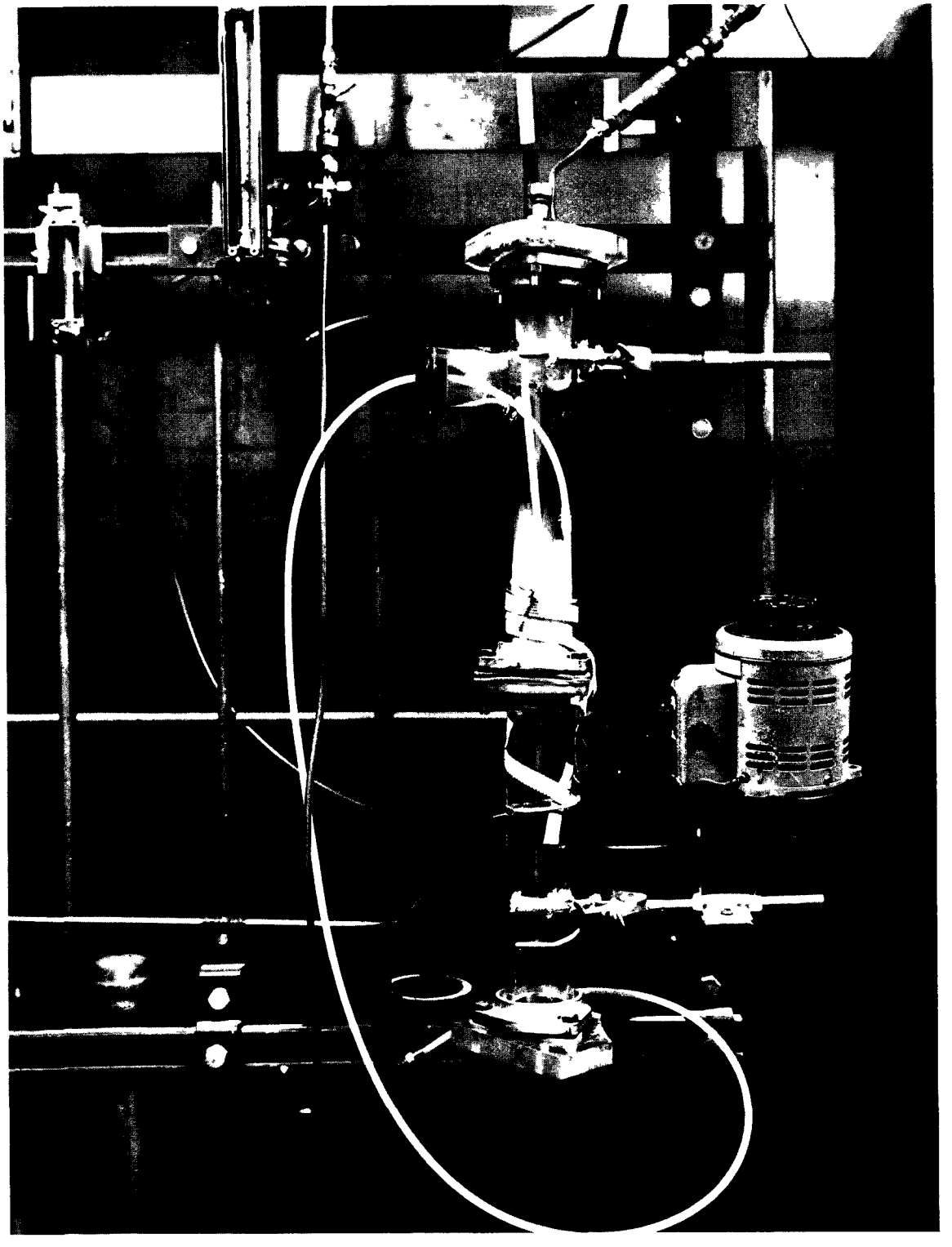

Figure 34. Photograph of the Two-inch Column and Auxiliary Equipment

pressure in the humidifiers. If the run was to be made at an elevated temperature, the Variac was set to give the desired temperature within the bed. Each run lasted approximately 24 hours and was terminated when the dew point of the air leaving the fluidized bed was equal to the dew point of the air entering the bed. At this point the bed temperature was recorded and a sample of the saturated gel was removed from the column. A three or four gram sample was weighed and placed in an oven at 220 ^{o}C. After 24 hours at this temperature the sample was removed and again weighed. The equilibrium water content of the gel (expressed as weight percent water vapor adsorbed on a dry gel basis) was then determined.

To evaluate the effect of absolute pressure upon the equilibrium water content of the gel a slightly different procedure was used. In this case the dew point of the gas leaving the fluidized bed at atmospheric pressure, p_1, was determined. Then the pressure was increased to p_2 and the new dew point noted. Using the equilibrium curves for atmospheric pressure, the change in water content of the gel (at equilibrium) was determined for the change in pressure from atmospheric to p_2. For a given dew point (the average of that at p_1 and p_2) and bed temperature, the effect of pressure was then expressed as the change in the equilibrium water percentage divided by the gauge pressure -- $\Delta\%$/psig.

3. Discussion of the Results

Figure 35 is a graph of equilibrium water content versus gel temperature with the air dew point as a parameter. The solid lines are from experimental data obtained in this work. The dotted lines represent data supplied by the Davison Chemical Co.[4]

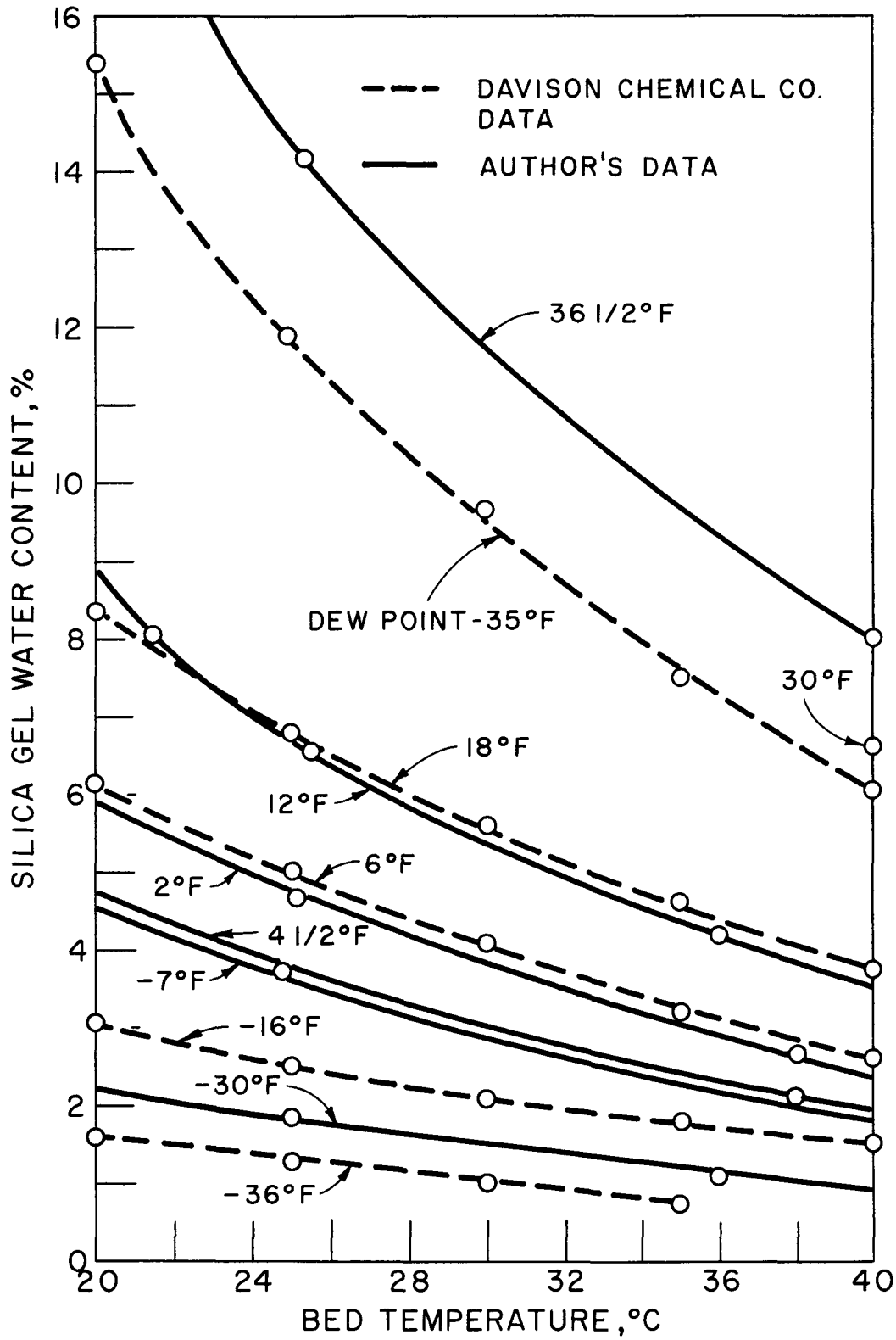

Figure 35. Equilibrium Silica Gel Water Content vs Bed Temperature with Dew Point as the Parameter

in their silica gel literature. It can be seen that the adsorptive capacity of the silica gel used in this work was effected by temperature in the same manner as was that used in the Davison experiments. However, as Figure 36 shows, the gel used in this work had a consistantly greater equilibrium water capacity, for any given humidity and bed temperature, than the material used to obtain the Davison data. This is quite reasonable in view of the fact that the Davison data is representative of many sizes and grades of gel available, and does not specifically apply to the material being used in this study.

A plot of the equilibrium curves for silica gel at atmospheric pressure for temperatures from 20 to 40°C is presented in Figure 37. In this figure the circled points represent actual experimental data obtained as outlined in the procedure. The portions of the figure not represented by actual experimental data were obtained by cross-plotting Figure 35.

In order to use one set of equilibrium curves based upon atmospheric pressure it was necessary to determine a correction factor to apply to the experimentally determined gel water contents obtained at pressures other than atmospheric. This correction factor -- change in equilibrium water percentage per psig -- was found to be a function of the bed temperature and the air dew point. Figure 38 shows the relationship between these variables. In this figure the lines for bed temperatures of 26, 28 1/2, 32, and 36°C were experimentally determined. The lines for other temperatures were then added on the basis of a logarithmic variation of bed temperature with the correction factor. A sample calculation showing

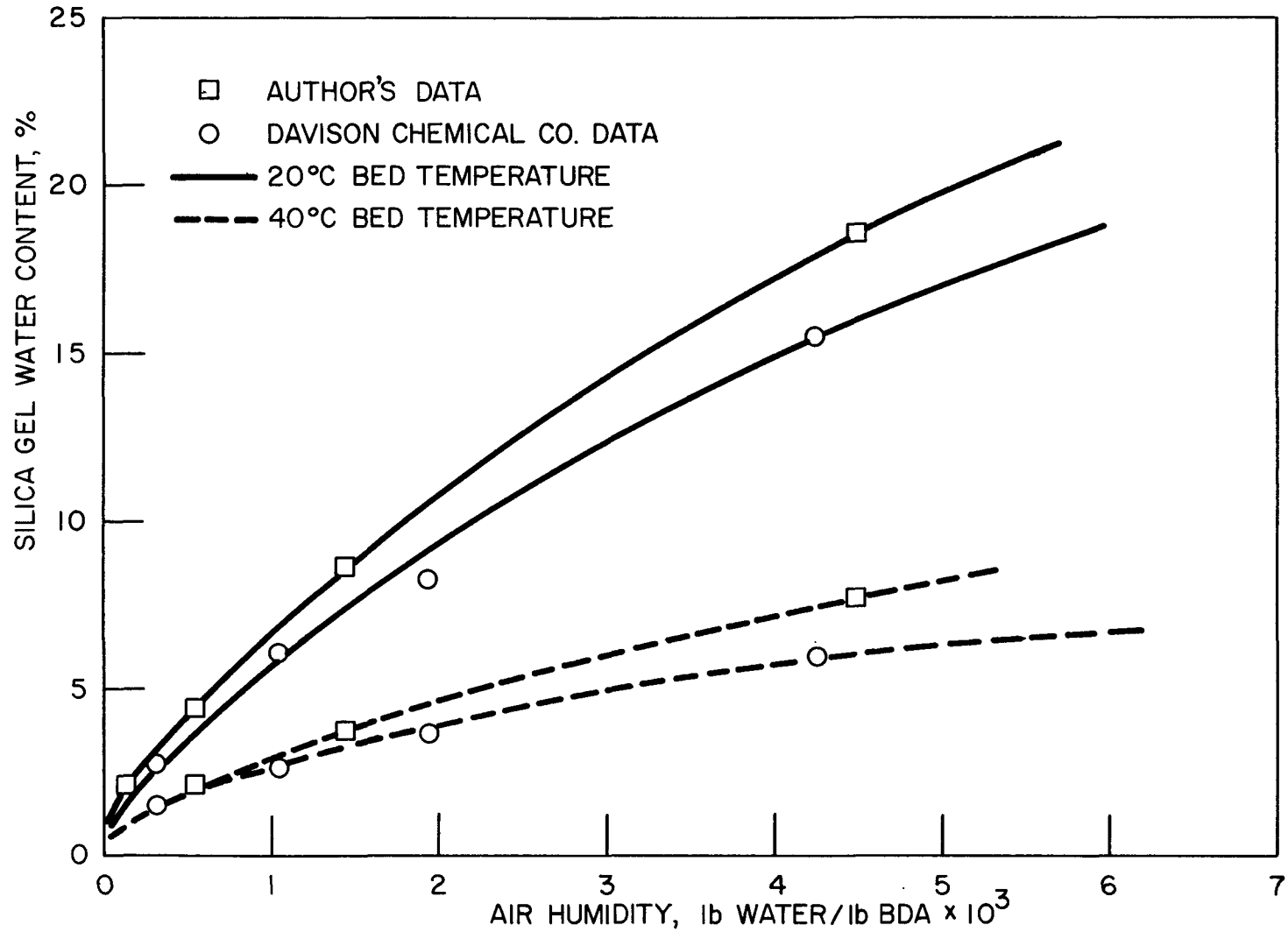

Figure 36. Comparison of Equilibrium Data Supplied by the Davison Chemical Co. with that Obtained in this Work.

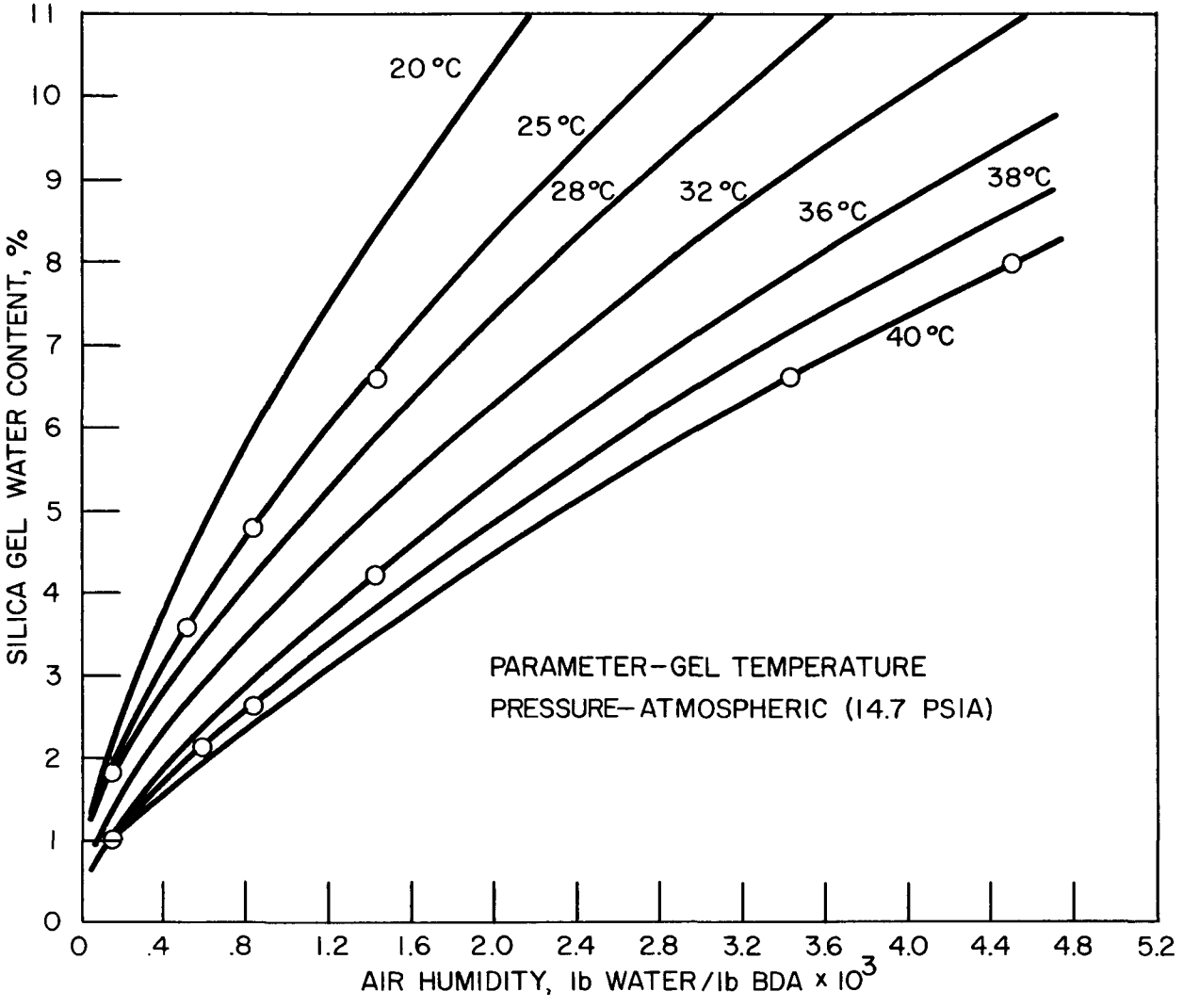

Figure 37. Equilibrium Silica Gel Water Content as a Function of the Air Humidity

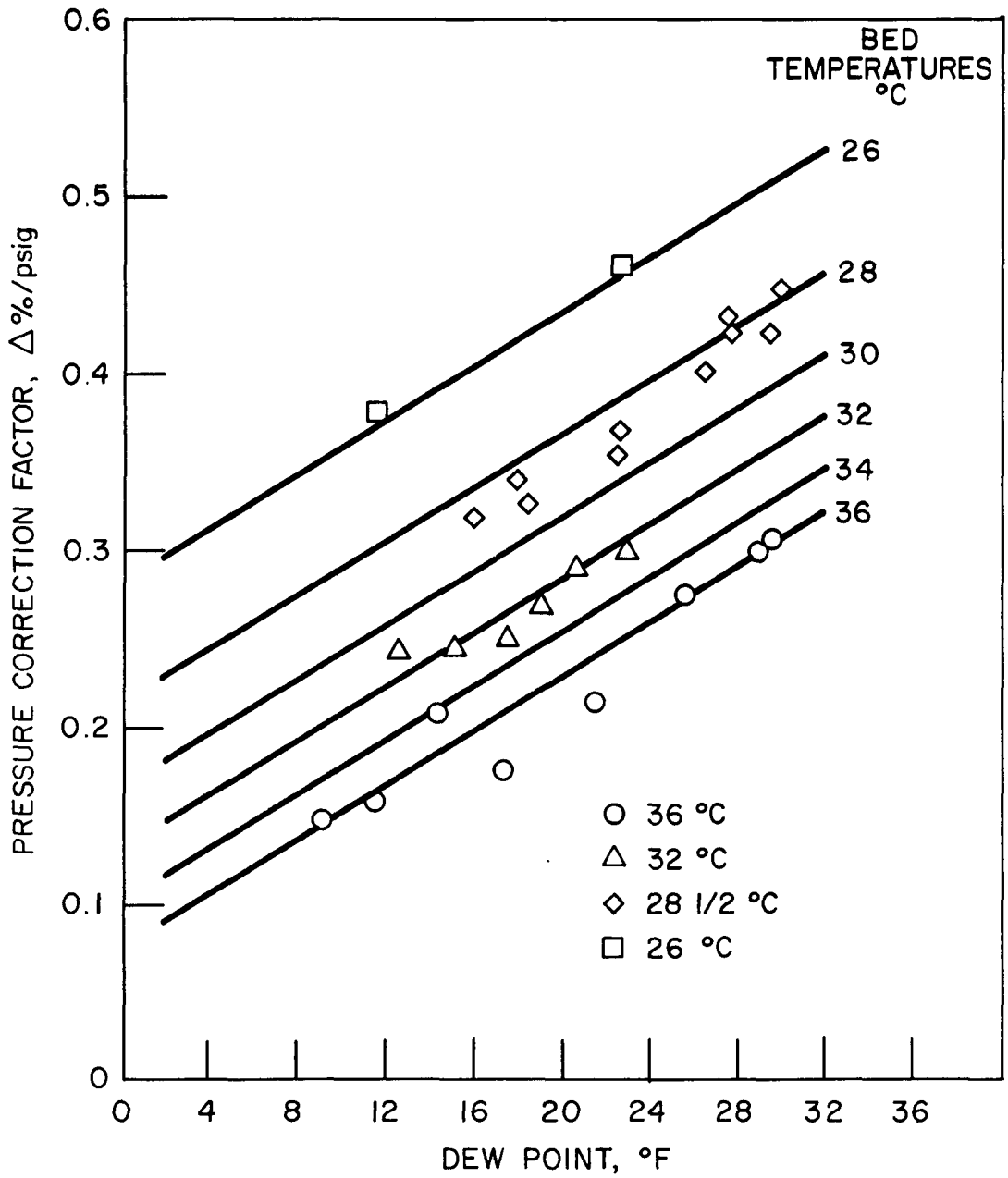

Figure 38. Pressure Correction Factor vs Dew Point with Bed Temperature as the Parameter

how $\Delta\%$/psig was calculated from experimental data is presented in Appendix II. All of the experimental data for this part of the thesis are also found in Appendix II.

D. Multistage Column Experiments

1. Equipment Modifications and Operating Conditions

Several minor changes were made in the multistage column for this study. First, on each of the three stages a Tygon tube (1/4-in. I.D.) was run from a point approximately 1/2 in. above the cover plate upward and to the outside of the column through a port in each of the brass sections. These tubes were used to obtain samples of the silica gel from the beds. Second, a thermometer was placed in each of the beds. These were attached to the vibration-transmitter rods (see Figure 3). Third, a piece of rubber hose was used to connect an opening in the top of the feed hopper to a line located in the top of the column. Through this hose the pressure was equalized between the feed hopper and the top of the column. Such a pressure equalization was necessary to insure a constant feed rate at high superficial air velocities. Fourth, one of the stainless steel filters was removed from one of the two gas outlets. It was replaced by a copper line which led from the gas outlet to a ventilated hood. Any solids carry-over was then trapped in the hood. This change was made to eliminate the necessity of blowing back the filters as the pressure built up due to trapped fines. The presence of any blow-back air would dilute the air leaving the top stage and lead to false dew point readings. Fifth, copper tubing was run from a point on the center line of the column located approximately twelve inches above the cover plate for each

stage to the dew point recorder. This permitted continuous determination of the dew point of the air leaving each stage.

The silica gel used for this work was a mixture consisting of particles from 28 to 200 mesh with an average weight-mean diameter of 0.0109-in. Three millimeter diameter inert glass beads were incorporated into each of the three stage supports.

2. Procedure

The silica gel as received from the Davison Chemical Company could easily lower the air dew-point from 60°F to -75°F. However, under these conditions the gel particles stuck to the sides of the glass column and to the inert beads in the support section, thus preventing solids throughput. It was noted that partially-saturated gel (the treated air leaving the bed had a dew point greater than -10°F) did not stick to the walls of the column. For this reason all of the feed material was partially saturated to the point where the air leaving the fluidized bed had a dew point of 0°F. The partial saturation of the gel was done in the top stage of the multistage column. The fluidizing air had a dew point of approximately 60°F before entering the bed at a superficial velocity of 0.20 ft/sec. The exit dew point was continuously monitored and when it reached 0°F the air was turned off and the column was emptied. The material was then stored in closed metal containers until the amount required to make a run had been prepared (approximately 24 lb).

Prior to starting a run the column was loaded with silica gel by the method described in Part 1. The moist fluidizing air was then adjusted to give the desired superficial air velocity,

the screw feeder turned on and the level-control system set to maintain the desired bed depth. In some runs the bed-level control system was operated manually in order to maintain a minimum (less than 1/4 in.) fluctuation in the bed depth. The column operating pressure was noted every 10 to 15 minutes. In all runs solids sampling and dew point measurement were done on the top stage first and the bottom stage last. This sequence was followed so that the air of lowest dew point (that leaving the top stage) went through the dew point equipment first. This resulted in faster dew point determinations because no time was lost in drying the lines. No samples were taken from a particular stage until the bed temperature and dew point remained constant. When these criteria were met, solids were removed from the stage in question and the dew point and bed temperature were recorded. A three to four gram sample of the solids was then weighed and placed in an oven at 220°C for 24 hours. The sample was then reweighed and its water content determined by weight difference. The water content of the gel (corrected for the effect of column pressure) combined with the equilibrium curve and the dew point of the air leaving each stage was then used to calculate the Murphree vapor efficiency. This process was repeated for the middle and bottom stages.

3. Theory

An evaluation of the efficiency of gas-solids contacting in a fluidized bed can be made by use of the Murphree vapor efficiency concept[25]. This concept was first developed for use in rectification. It is readily adaptable to fluidization for two reasons: (1) In the fluidized bed there is considerable turbulence

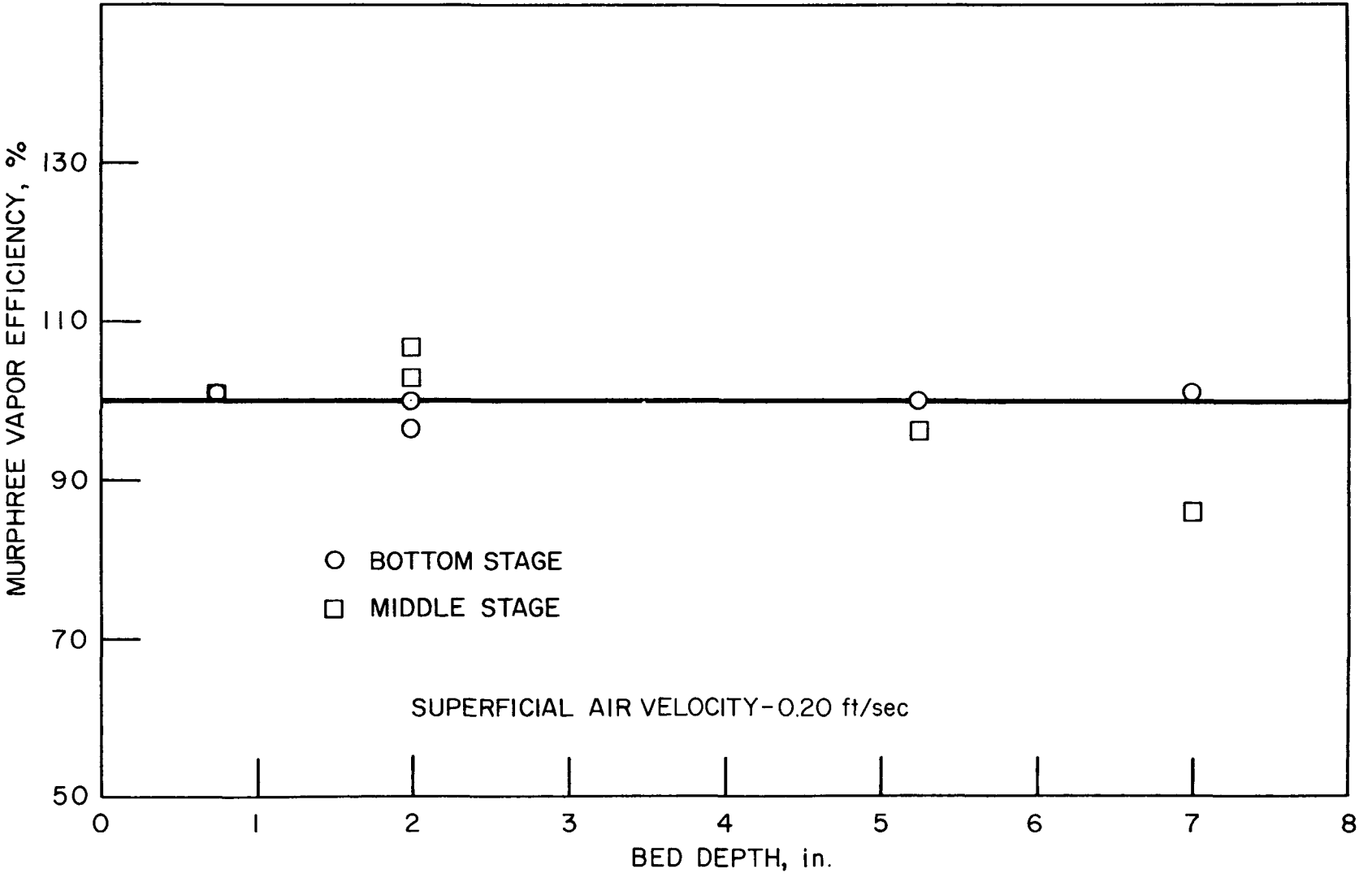

Figure 39. Murphree Vapor Efficiency vs Bed Depth

t = vibrator on-time, %

u = superficial vapor velocity, ft/sec

u_m = superficial vapor velocity at the maximum throughput rate, ft/sec

W = ball weight, lb

w = desired throughput rate of feed material at vapor velocity u, inert bead depth L, and vibrator on-time t, lb/hr

w_L^u = desired throughput rate of feed material at vapor velocity u, inert bead depth L, and vibrator on-time t, lb/sec

$W_L^{u_m}$ = throughput rate based upon the density of glass beads at vapor velocity u, and inert bead depth L, (t = 100%), lb/hr

W_L^u = throughput rate based upon the density of glass beads at vapor velocity u, and inert bead depth L, (t = 100%), lb/hr

Y_n = moisture content of the air leaving stage n, lb water/lb BDA

Y_n^* = moisture content of the air in equilibrium with the solids on plate n, lb water/ lb BDA

Y_{n+1} = moisture content of the air leaving stage n+1, lb water/lb BDA

A', X, Y = constants

ρ = bulk density of the feed particles, g/cc

ρ_g = density of the fluidizing gas, lb/ft^3

ρ_p = absolute density of the feed particles, lb/ft^3

ρ_{gl}^b = bulk density of the glass beads, 1.5 g/cc

ϕ_s = shape factor, dimensionless

BIBLIOGRAPHY

1. Campbell, J. R., Rumford, J., J. Soc. Chem. Ind., 69, 373 (1950).

2. Chu, J. C., Kalil, J., and Wetteroth, W. A., Chem. Eng. Progr., 49, 141 (1953).

3. Cox, M., Trans. Instn. Chem. Engrs., 36, 29 (1958).

4. Davison Chemical Co., Technical Bulletin 202, (1958).

5. Dotson, J. M., A.I.Ch.E. Journal, 5, 169 (1959).

6. Ermenc, E. D., Chem. Eng. Progr., 52, 488 (1956).

7. Ethering, L. D., Fritz, R. J., Nicholson, E. W., and Scheeline, H. W., Chem. Eng. Progr., 52, 274 (1956).

8. Evans, G. C., and Gerald, C. F., Chem. Eng. Progr., 49, 135 (1953).

9. Hancock, R. T., Mining Mag., 55, 90 (1936).

10. Jonke, A. A., Levitz, N. M., Litty, A., and Lawroski, S., Ind. Eng. Chem., 50, 1739 (1958).

11. Jonke, A. A., Argonne National Laboratory, personal communication.

12. Kettenring, K. N., Manderfield, E. L., and Smith, J. M., Chem. Eng. Progr., 46, 139 (1950).

13. Lemlich, R., and Caldas, I., A.I.Ch.E. Journal, 4, 376 (1958).

14. Leva, M., Grimmer, M., Weintraub, M., and Pollchik, M., Chem. Eng. Progr., 44, 511 (1948).

15. Ibid, 44, 707 (1948).

16. Levey, Jr., R. P., de la Garza, A., Jacobs, S. C., Heidt, H. M., and Trent, P. E., Union Carbide Nuclear Report No. Y-1233, Oak Ridge, Tenn.

17. Lewis, W. K., Gilliland, E. R., and Bauer, W. C., Ind. Eng. Chem., 41, 1104 (1949).

18. Lewis, W. K., Gilliland, E. R., and Glass, W., A.I.Ch.E. Journal, 5, 419 (1959).

38. Yasui, G., and Johanson, L. N., A.E.Ch.E. Journal, 4, 387 (1958).

39. Zenz, F. A., Othmer, D. F., "Fluidization and Particle Size Systems", Reinhold Publishing Corp., New York, (1960).

APPENDIX I

DESIGN STUDY

Specifications for the Feed Materials

Feed Material	Feed No.	Average Diameter, in.	Percent Retained on U. S. Sieves U. S. Sieve No. 40	50	60	70	80	100	120	140	170	200	230	400
Glass Beads	090	0.0110	-	-	80	-	20	-	-	-	-	-	-	-
	100	0.0080	-	-	-	-	85	15	-	-	-	-	-	-
	110	0.0058	-	-	-	-	5	75	20	-	-	-	-	-
	120	0.0045	-	-	-	-	-	-	20	70	10	-	-	-
	130	0.0039	-	-	-	-	-	-	-	10	50	35	5	-
	140	0.0033	-	-	-	-	-	-	-	-	10	60	20	10
	150	0.0030	-	-	-	-	-	-	-	-	-	5	50	45
	500	0.0069	-	2	-	20	-	37	-	24	-	16	-	1
Alumina	-	0.0045	-	-	-	-	-	1	-	58	-	39	-	2
Silica Gel	-	0.0109	11	38	-	14	-	15	-	10	-	8	-	4

Glass Beads: $\rho = 1.50$ g/cc, $\rho_p = 156$ lb/ft^3

Alumina: $\rho = 0.875$ g/cc, $\rho_p = 100$ lb/ft^3

Silica Gel: $\rho = 0.720$ g/cc, $\rho_p = 75$ lb/ft^3

Experimental Data for Vibrational Frequency Study

Data for Figures 9 and 10.

The throughput data for Figures 9 and 10 were obtained from Figures 6 and 7. The physical properties of the vibrators used to calculate the centrifugal force, F_c , are given in Figure 8.

Vibrator No.	t, %	S, CPM	F_c, lb (Fig. 9)	Energy per Unit Vibrator Weight, (in.-lb)/lb (Fig. 10)	w, lb/hr
10	25	7000	4.35	18.9	2.0
10	25	7500	5.00	21.6	6.8
10	25	9000	7.20	31.2	8.6
10	25	10000	8.88	38.4	10.0
13	25	6000	9.70	16.8	1.7
13	25	8000	17.2	29.8	8.5
13	25	9000	21.8	37.8	10.0
13	25	10000	26.9	46.6	12.5
10	50	7500	5.00	21.6	14.2
10	50	9000	7.20	31.2	18.0
10	50	10000	8.88	38.4	20.0
13	50	8000	17.2	29.8	16.8
13	50	9000	21.8	37.8	20.0
13	50	10000	26.9	46.6	24.5
10	75	7500	5.00	21.6	21.3
10	75	9000	7.20	31.2	27.3
10	75	10000	8.88	38.4	30.0
13	75	8000	17.2	29.8	25.3

Experimental Data for Vibrational Frequency Study

Data for Figures 9 and 10. (Concluded)

Vibrator No.	t, %	S, CPM	F_c, lb (Fig. 9)	Energy per Unit Vibrator Weight, (in.-lb)/lb (Fig. 10)	w, lb/hr
13	75	9000	21.8	37.8	30.0
13	75	10000	26.9	46.6	36.7
10	100	7500	5.00	21.6	28.5
10	100	9000	7.20	31.2	36.6
10	100	10000	8.88	38.4	40.0
13	100	8000	17.2	29.8	33.8
13	100	9000	21.8	37.8	40.0
13	100	10000	26.9	46.6	48.8

Experimental Data for Contactor Study

Data for Figure 12.

$u = 0.19$ ft/sec

$D_p = 0.0039$ in. (No. 130)

$D_I = 0.0357$ in.

$L = 0.218$ in.

$H = 7$ in.

Run No.	Contactor No.	Vibrator No.	S, CPM	t, %	w, lb/hr
I231	300	10	10000	25	9.2
I232	300	10	10000	48	20.0
I233	300	10	10000	79	31.0
I221	301	13	11000	39	12.3
I220	301	13	11000	52	15.6
I223	301	13	11000	88	25.0
I300	302	10	7500	22	8.4
I301	302	10	7500	53	18.7
I302	302	10	7500	91	31.6
I305	303	10	8300	34	16.4
I304	303	10	8300	68	37.5
I303	303	10	8300	86	47.5
I306	304	10	8000	21	11.8
I307	304	10	8000	46	23.3
I308	304	10	8000	68	35.7

Experimental Data for Plate Resistance Study

Data for Figures 17 and 18.

Contactor No. 303
Vibrator No. 10 at 8000 CPM
u = 0.19 ft/sec

Figure No.	Run No.	D_p and Feed No., in.	t, %	w, lb/hr
17	I508	0.0058 (No. 110)	88	10.5
(L = 0.144 in., D_I = 0.0357 in.)	I506	0.0045 (No. 120)	42	15.0
	I507	0.0045	83	29.8
	I500	0.0039 (No. 130)	22	16.3
	I501	0.0039	61	42.9
	I502	0.0039	70	48.8
	I503	0.0030 (No. 150)	20	19.5
	I504	0.0030	53	46.3
	I505	0.0030	72	61.0
18	I519	0.0058 (No. 110)	100	27.3
(L = 0.072 in., D_I = 0.0357 in.)	I512	0.0045 (No. 120)	23	17.5
	I513	0.0045	53	33.8
	I514	0.0045	100	71.0
	I509	0.0039 (No. 130)	21	28.0
	I510	0.0039	55	63.6
	I511	0.0039	100	111
	I515	0.0030 (No. 150)	19	36.0
	I516	0.0030	45	66.0
	I517	0.0030	100	127

Experimental Data for Plate Resistance Study

Data for Figure 19.

Contactor No. 303
Vibrator No. 10 at 8000 CPM
D_p = 0.0039 in. (No. 130)
u = 0.19 ft/sec

Run No. or Other Source	Energy per Unit Vibrator Weight, (in.-lb)/lb	Column Free Area, ft^2	Number of Inert Bead Layers	W_L^u, lb/hr
I521	25	0.059	0	360
Theory	(25)	0.042	1	258
Theory	(25)	0.021	2	129
Theory	(25)	0.0105	3	64
Theory	(25)	0.0052	4	32
Theory	(25)	0.0026	5	16
Theory	(25)	0.0013	6	8
Theory	(25)	0.0006	7	4
Theory	(25)	0.0003	8	2
I511	25	—	2.3	111
I500-502	25	—	4.5	71
I303-305	25	—	6.8	54
From Fig. 10	31	—	6.8	83*
From Fig. 10	50	—	6.8	108*

* Corrected for contactor efficiency.

Experimental Data for Plate Resistance Study

Data for Figure 20.

Data for this figure were obtained by averaging the increase or decrease in the throughput rate for several runs as a function of the inert-bead depth. The throughput rate occurring with an inert-bead depth of 0.218 in. was used as the basis.

L, in.	Change in the Throughput Rate lb/hr	S', lb/hr
0.436	-21.5	100 - 21.5 = 78.5
0.218	0	100 + 0 = 100
0.144	+11	100 + 11 = 111
0.072	+50	100 + 50 = 150

Experimental Data for Plate Resistance Study

Data for Figures 21 and 22.

Contactor No. 303
Vibrator No. 10 at 8000 CPM
u = 0.19 ft/sec
H = 7 in.

Figure No.	Run No.	D_p and Feed No., in.	t, %	w, lb/hr
21	I541	0.0045 (No. 120)	28	16.1
(Copper inert beads, L = 0.072 in.)	I537	0.0045	49	19.5
	I538	0.0045	53	28.3
	I540	0.0045	64	31.2
	I539	0.0045	100	48.5
	I535	0.0039 (No. 130)	0	6.2
	I534	0.0039	31	35.0
	I535	0.0039	49	52.2
	I536	0.0039	100	110
22	I528	0.0045 (No. 120)	50	8.6
(Alumina inert beads, L = 0.144 in.)	I531	0.0045	100	18.2
	I532	0.0039 (No. 130)	60	20.4
	I533	0.0039	100	31.9

Experimental Data for Plate Resistance Study

Data for Figure 23.

Run No.	u, ft/sec	D_I, in.	L, in.	D_p and Feed No., in.	t, %	w, lb/hr
I525	0.35	0.118	0.436	0.0110 (No. 090)	100	142
I526	0.21	0.118	0.436	0.0080 (No. 100)	0	17.2
I526	0.21	0.118	0.436	0.0080	100	292
I544	0.38	0.0592	0.218	0.0080	48	17.8
I542	0.38	0.0592	0.218	0.0080	80	27.2
I543	0.38	0.0592	0.218	0.0080	100	37.5
I545	0.19	0.0592	0.218	0.0045 (No. 120)	0	2.8
I545	0.19	0.0592	0.218	0.0045	25	37.8
I546	0.19	0.0592	0.218	0.0045	47	65.6
I547	0.19	0.0592	0.218	0.0045	58	86.0
I550	0.19	0.0592	0.218	0.0069 (No. 500)	32	19.9
I548	0.19	0.0592	0.218	0.0069	53	34.2
I549	0.19	0.0592	0.218	0.0069	100	70.4

Experimental Data for Bed Depth Study

Data for Figures 24 and 25. (Penn State data from reference 37.)

Contactor No. 303

Vibrator No. 10 at 8000 CPM

D_p = 0.0039 in. (No. 130)

u = 0.19 ft/sec

D_I = 0.0357 in.

L = 0.144 in.

Figure No.	Run No.	H, in.	t, %	w, lb/hr
24	I909	3	41	18.9
	I908	3	76	38.5
	I910	3	100	53.0
	I911	5	47	26.0
	I912	5	78	42.2
	I913	5	100	53.5
	I916	7	24	15.2
	I915	7	46	28.2
	I914	7	84	50.0
	I919	9	32	17.7
	I918	9	48	26.2
	I917	9	64	37.5
	I920	9	82	46.6
25	I908-910	3	100	49
	I911-913	5	100	55
	I914-916	7	100	60
	I917-920	9	100	60

Experimental Data for Superficial Air Velocity Study

Data for Figures 26, 27 and 28.

Contactor No. 303

Vibrator No. 10 at 8000 CPM

H = 7 in.

t = 100%

Figure No.	Run No.	u, ft/sec	W_L^u, lb/hr
26	I819	0	48.0
(L = 0.144 in., D_I = 0.0357 in., D_p = 0.0039 in.)	I823	0.074	72.0
	I814-817	0.11	66.0
	I500-502	0.19	69.0
	I820-822	0.15	73.0
	I801-805	0.27	53.0
	I806-807	0.35	37.5
	I808-811	0.42	33.0
27	I831	0	14.5
(L = 0.218 in., D_I = 0.0592 in., D_p = 0.0080 in.)	I828	0.11	19.8
	I830	0.13	43.4
	I829	0.15	58.8
	I825	0.19	55.0
	I824	0.23	50.0
	I846	0.34	38.0
	I826	0.43	26.4
	I827	0.50	25.8

Continued on next page.

Experimental Data for Uncontrolled Throughput Study

Data for Figure 30.

Data for this figure were determined from an overall analysis of the experimental data. The coordinates for the points shown are given below.

L, in.	$D_c - D_p \phi_s$, in.
0.072	0.0019
0.144	0.0031
0.436	0.0071

Experimental Data for the Design Correlation

Data for Figure 31.

Feed	ρ, g/cc	ρ_p, lb/ft^3	ϕ_s,	L, in.	D_c, in.x10^4	$D_p\phi_s$, in.x10^4	u, ft/sec	u_m, ft/sec	w_L^u, lb/hr	(127)x (u-u_m), ft/sec	$W_{.218}^u$ lb/hr	$W_{.218}^{u_m}$ lb/hr	$D_c-D_p\phi_s$ in.x10^4
Glass	1.5	156	1	0.218	55	45	0.19	0.107	25.5	10.5	25.5	36	10
Glass	1.5	156	1	0.218	55	39	0.19	0.100	53.5	11.4	53.5	65	16
Glass	1.5	156	1	0.218	55	33	0.19	0.092	63.0	12.4	63.0	75	22
Glass	1.5	156	1	0.218	55	30	0.19	0.088	72.0	13.0	72.0	85	25
Glass	1.5	156	1	0.072	55	39	0.19	0.100	111	11.4	61.0	72	16
Glass	1.5	156	1	0.072	55	30	0.19	0.088	127	13.0	77.0	90	25
Glass	1.5	156	1	0.144	55	58	0.19	0.122	12.0	8.6	-3	6	-3
Glass	1.5	156	1	0.144	55	45	0.19	0.107	35.0	11.0	20.0	31	10

Continued on next page.

Experimental Data for the Design Correlation

Data for Figure 31. (Concluded)

Feed	ρ, g/cc	ρ_p, lb/ft^3	ϕ_s,	L, in.	D_c, in.x10^4	$D_p\phi_s$, in.x10^4	u, ft/sec	u_m, ft/sec	w_L^u, lb/hr	(127)x $(u-u_m)$, ft/sec	$W^u_{.218}$ lb/hr	$W^{u_m}_{.218}$ lb/hr	$D_c-D_p\phi_s$ in.x10^4
Glass	1.5	156	1	0.144	55	39	0.19	0.100	70.0	11.4	55.0	66	16
Glass	1.5	156	1	0.144	55	30	0.19	0.088	85.0	12.9	70.0	83	25
Glass	1.5	156	1	0.218	92	80	0.36	0.143	36.0	27.8	36.0	64	12
Glass	1.5	156	1	0.218	92	69	0.19	0.133	68.0	7.2	68.0	75	23
Glass	1.5	156	1	0.218	92	45	0.19	0.107	141	10.5	141	152	47
Glass	1.5	156	1	0.436	168	110	0.33	0.169	142	23.0	165	188	58
Alumina	0.875	100	1.62	0.218	92	73	0.15	0.072	33.4	10.0	57.0	67	19
Silica Gel	0.720	75	1.40	0.218	183	152	0.63	0.096	45.6	16.5	93.0	110	31

Comparison of the Experimental and Calculated Throughput Rates using the Design Correlation

Feed	$D_c - D_p \phi_s$ in. x 10^4	$W^{u_m}_{.218}$ lb/hr	L, in.	$W^{u_m}_L$ lb/hr	$(127)x(u-u_m)$ ft/sec	W^u_L lb/hr	ρ, g/cc	t, %	w^u_L Calc. lb/hr	w^u_L Expt. lb/hr	Calc.- Expt. lb/hr
Glass	10	43.3	0.218	43.3	10.5	32.8	1.5	100	32.8	25.5	+ 7.3
Glass	16	61.1	0.218	61.1	11.4	49.7	1.5	100	49.7	53.5	- 3.8
Glass	22	78.9	0.218	78.9	12.4	66.5	1.5	100	66.5	63.0	+ 3.5
Glass	25	87.8	0.218	87.8	13.0	74.8	1.5	100	74.8	72.0	+ 2.8
Glass	16	61.1	0.072	111.1	11.4	99.7	1.5	100	99.7	111.0	-11.3
Glass	25	87.8	0.072	137.8	13.0	124.8	1.5	100	124.8	127.0	- 2.2
Glass	-3	4.8	0.144	19.8	8.6	11.2	1.5	100	11.2	12.0	- 0.8
Glass	10	43.3	0.144	58.3	10.5	47.8	1.5	100	47.8	35.0	+12.8

Continued on next page.

Comparison of the Experimental and Calculated Throughput Rates using the Design Correlation (Conclusion)

Feed	$D_c - D_p \phi_s$ in. x 10^4	$W^{u_m}_{.218}$ lb/hr	L, in.	$W^{u_m}_L$ lb/hr	$(127)x(u-u_m)$ ft/sec	W^u_L lb/hr	ρ, g/cc	t, %	w^u_L Calc. lb/hr	w^u_L Expt. lb/hr	Calc.- Expt. lb/hr
Glass	16	61.1	0.144	76.1	11.4	64.7	1.5	100	64.7	70.0	- 5.3
Glass	25	87.8	0.144	102.8	12.9	89.9	1.5	100	89.9	85.0	+ 4.9
Glass	12	49.4	0.218	49.4	27.8	21.6	1.5	100	21.6	36.0	- 4.4
Glass	23	81.8	0.218	81.8	7.2	74.6	1.5	100	74.6	68.0	+ 6.6
Glass	47	153.0	0.218	153.0	10.5	142.5	1.5	100	142.5	141.0	+ 1.5
Glass	58	186.0	0.436	163.0	23.0	140.0	1.5	100	140.0	142.0	- 2.0
Alumina	19	70.0	0.218	70.0	10.0	60.0	0.875	100	35.0	33.4	+ 1.6
Silica Gel	31	103.0	0.218	103.0	16.5	86.5	0.720	100	42.0	45.6	- 3.6

Rotameter Correction Equation

In order to correct the observed rotameter readings to flow rates for 14.7 psia and 70°F, the observed readings were multiplied by the following correction factor:

$$\sqrt{(530/T_r)\ (P_r/14.7)} \quad = \quad \sqrt{36\ P_r/T_r}$$

In this equation T_r is the absolute temperature (°R) of the air flowing through the meter and P_r the pressure (psia) at which the air is being metered. This factor was determined from data supplied by the Brooks Rotameter Company. With the experimental conditions used in this study, the correction factor never exceeded 10% and was generally less than 5% of the observed reading.

Derivation of the Vibrator Centrifugal Force Equation

The general centrifugal force equation for a revolving steel ball is:

$$F_c = \frac{W}{g_c}(R\omega^2) \qquad (1)$$

where W is the ball weight in lb; R the path radius of curvature; g_c the gravitational constant (32.2 ft/sec^2); ω the angular velocity; and F_c the centrifugal force in lb_f. The angular velocity is defined as:

$$\omega = V/R \qquad (2)$$

in which V is the peripheral velocity, ft/sec. Substituting (2) into (1) gives:

$$F_c = \frac{W}{g_c}(R)(V^2/R^2) = \frac{WV^2}{g_cR} \qquad (3)$$

Since V in terms of revolutions per minute, S , is:

$$V = \frac{2\pi R}{60}(S) \qquad (4)$$

We find that:

$$F_c = \frac{W}{g_c} \times \frac{2^2\pi^2R^2S^2}{60R} = 0.000341\,WRS^2 \qquad (5)$$

If R is given in inches then (5) becomes:

$$F_c = 2.84 \times 10^{-5}\,WRS^2 \qquad (6)$$

Equation 6 is the centrifugal force equation used in this study.

Derivation of the Critical Diameter Concept

The "critical diameter", D_c , is defined as the diameter of the largest sphere that will pass through the void space between the tightly packed inert beads. The relationship between these two diameters can be derived from Figure A.

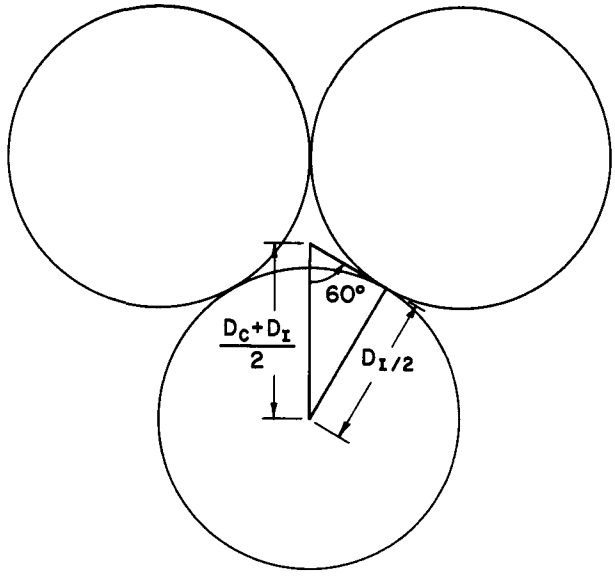

From trigometric considerations:

$$\sin 60^\circ = \frac{D_I}{2} \div \frac{D_c + D_I}{2} = \frac{D_I}{D_c - D_I} = 0.868$$

Solving the above equation for D_I gives the desired equation, namely:

$$D_I = \frac{0.868}{0.134} D_c = 6.46\ D_c$$

Relationship Between the Inert Bead Layers and the Inert Bead Depth

Assuming close packing, the spherical beads will aline themselves as shown below.

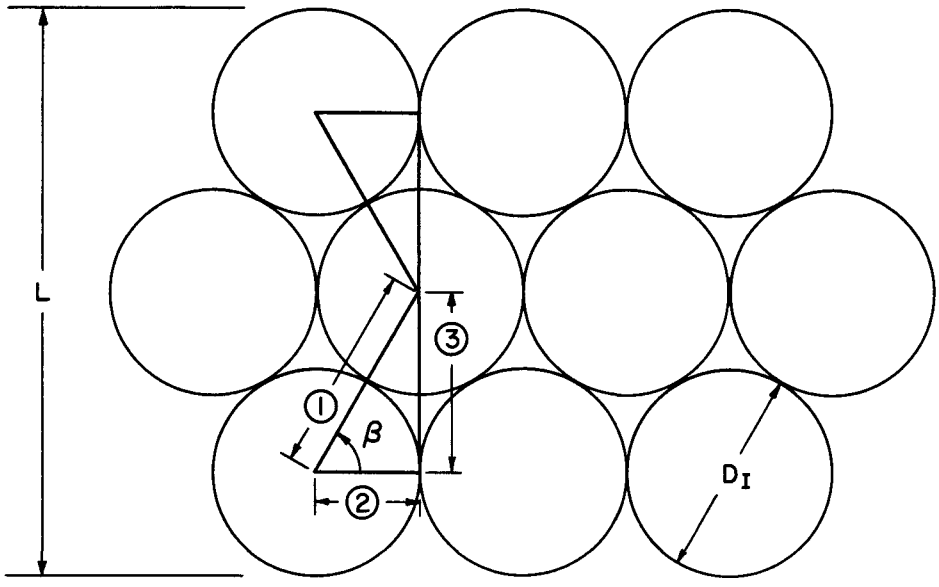

The total depth of inert beads, L , for the three layers shown will be less than three times the particle diameter, D_I. In the triangle shown above:

$$(1) = D_I$$

$$(2) = D_I/2$$

And from trigonometry with $\beta = 60^\circ$:

$$\sin \beta = (3)/D_I = \sin 60^\circ$$

From which:

$$(3) = D_I(\tfrac{1}{2}\sqrt{3}) = 0.868(D_I)$$

From the figure we see that if x equals the total number of bead layers in a 'bed' of depth L then:

$$L = D_I + 0.868(D_I)(x - 1)$$

Relationship Between the Inert Bead Layers and the Inert Bead Depth
(Concluded)

Therefore for beads with a diameter (D_I) of 0.0357 inches:

L, in.	x, layers
0.218	6.8
0.144	4.5
0.072	2.2

APPENDIX II

MASS-TRANSFER STUDY

Experimental Equilibrium Data

Data for Figure 35.

Run No.	Dew Point °F	Sample Wet Wt., gm	Sample Dry Wt., gm	Gel Water Content, %
E21	-30	3.6438	3.6070	1.02
E20	-30	2.4248	2.3793	1.92
E19	- 7	3.5442	3.4154	3.77
E18	- 4 1/2	3.1457	3.0790	2.17
E17	+ 2	3.1551	3.0158	4.62
E16	+ 2	3.0206	2.9418	2.68
E15	+12	2.7863	2.6750	4.20
E4	+12	3.4622	3.2478	6.60
E14	+12	4.1697	3.8575	8.09
E2	+36 1/2	1.7888	1.5650	14.3
E22	+36 1/2	2.9265	2.7122	7.90
E23	+30	2.5743	2.4147	6.60
*	-36	--	--	0.70
*	-36	--	--	1.6
*	-16	--	--	1.5
*	-16	--	--	3.0
*	+ 6	--	--	2.6
*	+ 6	--	--	6.1
*	+18	--	--	3.7
*	+18	--	--	8.3
*	+35	--	--	6.0
*	+35	--	--	15.4

* Davison Data[4]

Experimental Equilibrium Data

Data for Figure 36.

Bed Temp., °C	Dew Point, °F	Humidity, lb/lbx10^3	Gel Water Content,%
20	-30	0.1464	2.2
20	- 7	0.5423	4.5
20	+12	1.454	8.8
20	+36 1/2	4.540	18.8
20	-16	0.3301	3.0 *
20	+ 6	1.074	6.1 *
20	+18	1.953	8.3 *
20	+35	4.275	15.4 *
40	- 7	0.5423	1.8
40	+12	1.454	3.6
40	+36 1/2	4.540	8.0
40	-16	0.3301	1.5 *
40	+ 6	1.074	2.6 *
40	+18	1.953	3.8 *
40	+35	4.275	6.0 *

* Davison Data (4)

Experimental Equilibrium Data

Data for Figure 37.

Run No.	Bed Temp., ^{o}C	Dew Point, ^{o}F	Humidity, $lb/lbx10^{3}$	Gel Water Content,%
E4	25	+12	1.454	6.6
E17	25	+ 1	0.8295	4.7
E19	25	- 7	0.5423	3.7
E20	25	-30	0.1464	1.9
E15	36	+12	1.454	4.2
E21	36	-30	0.1464	1.02
E16	38	+ 2	0.8739	2.68
E18	38	- 4 1/2	0.6205	2.17
E22	40	+36 1/2	4.540	7.9
E23	40	+30	3.454	6.6

Equilibrium Pressure Correction Data

Data for Figure 38.

Run No.	p, psig	Δpsig	Dew Point, °F	Dew Point Average, °F	Humidity, lb/lbx10^3	Gel Water Content, %	Δ%	Δ%/psig	Bed Temp., °C
PC1	0.70	2.55	27	25 1/2	3.00	7.05	0.70	0.275	36
	3.25		24		2.60	6.35			
PC2	0.75	2.50	30 3/4	29	3.57	7.90	0.75	0.300	36
	3.25		27 1/2		3.07	7.15			
PC3	3.60	2.85	28	29 3/4	3.15	7.25	0.87	0.305	36
	0.75		31 1/2		3.70	8.12			
PC4	0.80	2.45	13	11 1/2	1.53	4.30	0.40	0.163	36
	3.25		10		1.32	3.90			
PC5	3.25	2.45	13	14 1/2	1.53	4.30	0.51	0.208	36
	0.80		16		1.77	4.81			
PC6	3.60	2.80	19	20 1/2	2.05	5.35	0.60	0.214	36
	0.80		22		2.37	5.95			
PC7	0.87	2.38	11	9 1/2	1.38	4.05	0.35	0.147	36
	3.25		8		1.19	3.70			

Sample Calculation of the Equilibrium Pressure Correction Term from the Experimental Data

The following data were taken from a typical run.

Bed temperature: 28 1/2°C
Initial pressure in the column: 3.60 psig
Final pressure in the column: 0.45 psig
Initial dew point: 20 1/2°F
Final dew point: 24 3/4°F
Initial air humidity: 0.0022 lb water/lb BDA
Final air humidity: 0.0027 lb water/lb BDA

From the equilibrium curve (Figure 37) at 28 1/2 °C the equilibrium gel water content for the initial and final humidities was found to be:

Initial gel water content: 7.70%
Final gel water content: 8.85%

The difference in the gel water content, $\Delta\%$, is therefore 1.15%. The difference in column pressure was 3.15 psig. Therefore the pressure correction term, $\Delta\%/\text{psig}$, is 1.15/3.15 or 0.365 %/psig.

LIST OF TABLES

LIST OF FIGURES